Development of One-Step Chemistry Models for Flame and Ignition Simulation

S.P.M. Bane, J.L. Ziegler, and J.E. Shepherd

Graduate Aerospace Laboratories
California Institute of Technology
Pasadena, CA 91125

Abstract

This report describes the work done in collaboration with S. Dorofeev and C. Bauwens at FM Global Research on developing one-step chemistry models for use in flame, ignition, and large-scale combustion simulations. Methods based on constant pressure and constant volume explosion theory are developed to extract physically reasonable values of the effective reaction order and activation energy for a range of hydrogen-air mixtures. Using the calculated effective parameters, one-step chemistry models are developed and implemented in a one-dimensional flat flame code. The one-step models are adjusted such that the flame speed and temperature computed with the one-step model matches the values calculated using a detailed chemical mechanism. A model for stoichiometric hydrogen-air using a second order one-step reaction also accurately simulated the response of the flame to small changes in the initial temperature and pressure. A one-step model for a 15% hydrogen-air mixture is developed using four chemical species and realistic transport properties to accurately simulate the flame response to a strained flow field. The four-species one-step model for 15% hydrogen-air was implemented in CFD software and used to simulate a one-dimensional flat flame for comparison with previous computations. Two-dimensional axisymmetric simulations of spark discharge in a non-reacting gas and ignition in hydrogen were performed using the one-step chemistry model and the reacting Navier-Stokes equations with heat and mass diffusion.

Contents

List of Figures

List of Tables

1   Introduction

Determining the risk of accidental ignition of flammable mixtures is a topic of tremendous importance in industry and aviation safety. The concept of minimum ignition energy (MIE) has traditionally formed the basis for studying ignition hazards of fuels. Standard test methods for determining the MIE use a capacitive spark discharge as the ignition source (Babrauskas, 2003), and there have been extensive experimental studies to determine the minimum ignition energies of many different flammable mixtures. Work has been done on the numerical modeling of the hydrodynamic evolution following a spark discharge in a non-reactive gas (Kono et al., 1988; Ekici et al., 2007) and on spark ignition in reactive mixtures using various models for the flame and spark discharge (Kravchik et al., 1995; Thiele et al., 2000). However, due to the complexity of modeling the ignition process, predicting ignition remains primarily an experimental issue.

The objective of this work is to develop a numerical model of the spark ignition process that accurately captures both the chemistry and the fluid dynamics over a range of physical scales. We use the AMROC (Adaptive Mesh Refinement in Object-Oriented C++) software package developed by R. Deiterding (Deiterding, 2003) to solve the non-reactive and reactive Euler and Navier-Stokes equations including mass diffusion with high resolution. Preliminary 2D cylindrical computations of the flow field evolving from a spark discharge in a non-reactive gas have been completed.

To perform highly-resolved simulations quickly and with limited processing resources, simplified chemistry must be used. In this work we use the simplest possible chemistry, a one-step reaction model. One-step chemistry models are often used in large-scale simulations such as combustion in HCCI engines (e.g., (Hamosfakidis et al., 2009)), ramjet engines (e.g., (Roux et al., 2010)), and swirl gas combustors (e.g., (Grinstein and Fureby, 2005)), and in simulations involving turbulence such as turbulent flames (e.g., (Sankaran and Menon, 2005)). Work has been done recently at FM Global Research by Dorofeev and Bauwens (Bauwens, 2007) and also by Fernández-Galisteo et al. (Fernández-Galisteo et al., 2009) to develop one-step chemistry models for hydrogen-air mixtures, but no single scientific method exists for extracting physically reasonable parameters for one-step models.

Since early 2008, we have collaborated with Sergey Dorofeev and Carl Bauwens at FM Global Research on developing one-step models for hydrogen-air and methane-air mixtures. This report summarizes the work done between approximately February 2008 and June 2009 that has been presented in various unpublished reports. In this work we have developed methods based on thermal explosion theory for extracting physically reasonable effective activation energies and reaction orders for one-step models. We first implemented the one-step models into a steady 1D laminar flame code using Cantera software for chemically reacting flow (Goodwin, 2005) and validated the models by comparing the flame properties with those calculated using the full chemical mechanism. We then implemented our one-step model for stoichiometric hydrogen-air into the AMROC software to perform a preliminary simulation of a 1D laminar flame. The flame simulations in AMROC were validated using the flame calculations from Cantera, and the one-step model chemistry will be extended to non-steady and multidimensional simulations.

2   Constant Pressure Explosion Method

In this section we derive expressions for the effective activation energy and reaction order based on thermal explosion theory. The derivation of the effective reaction order is given in the first section and reaction orders for hydrogen-air mixtures are estimated using the results of constant pressure explosion computations performed with Cantera software (Goodwin, 2005). In the second section the derivation of the effective activation energy is presented and values of the activation energy for hydrogen-air mixtures are estimated using the calculated reaction orders and Cantera computations.

2.1   Estimating Effective Reaction Order

In a constant pressure explosion the enthalpy is also constant and can be expressed as a function of temperature and mass fraction

$$h = h\left(T, Y\right) . \tag{1}$$

Differentiating the enthalpy with respect to time relates the change in temperature to the change in mass fraction:

$$\frac{dh}{dt} = \frac{\partial h}{\partial T}\frac{dT}{dt} + \frac{\partial h}{\partial Y}\frac{dY}{dt}$$

$$= c_p\frac{dT}{dt} - q\frac{dY}{dt} = 0 \tag{2}$$

where q is the heat release per unit mass and

$$\frac{dY}{dt} = \frac{W\dot{\omega}}{\rho} \ . \tag{3}$$

The molar production rate of product per unit volume, $\dot{\omega}$, is assumed to have an Arrhenius form:

$$\dot{\omega} = A[O]^{n_O}[F]^{n_F}\exp\left(\frac{-E_a}{\widetilde{R}T}\right) \tag{4}$$

where $[O]$ and $[F]$ are molar concentrations of the oxidizer and fuel respectively, and n_O and n_F are empirical reaction orders. Using the ideal gas law, we can represent the concentration of a component i in terms of the density:

$$[i] = \frac{n_i}{V} = \frac{p_i}{\widetilde{R}T} = \frac{x_i p}{\widetilde{R}T} = \frac{x_i}{W_i}\rho \tag{5}$$

where p_i, x_i, and W_i are the partial pressure, mole fraction, and molar mass of component i, respectively. Using this definition of molar concentration in Equation 4 we obtain

$$\dot{\omega} = A\left[\frac{x_O}{W_O}\rho\right]^{n_O}\left[\frac{x_F}{W_F}\rho\right]^{n_F}\exp\left(\frac{-E_a}{\widetilde{R}T}\right)$$

$$= \left(A\frac{x_O^{n_O}x_F^{n_F}}{W_O^{n_O}W_F^{n_F}}\right)\rho^{n_O+n_F}\exp\left(\frac{-E_a}{\widetilde{R}T}\right) \tag{6}$$

and therefore

$$\frac{dY}{dt} = \frac{W\dot{\omega}}{\rho} = \left(AW\frac{x_O^{n_O}x_F^{n_F}}{W_O^{n_O}W_F^{n_F}}\right)\rho^{n_O+n_F-1}\exp\left(\frac{-E_a}{\widetilde{R}T}\right) \ . \tag{7}$$

If we define the effective activation energy n as $n = n_O + n_F$ and combine the terms in the parenthesis into a parameter Z, then the expression for the change in temperature versus time becomes:

$$\frac{dT}{dt} = \frac{q}{c_p}Z\rho^{n-1}\exp\left(\frac{-E_a}{\widetilde{R}T}\right) \ . \tag{8}$$

We now apply the Frank-Kamenetskii approximation by assuming a small temperature rise, i.e.,

$$T = T_0 + T' \tag{9}$$

where $T' \ll T_0$. Substituting this definition of temperature into Equation 8 gives

$$\frac{dT'}{dt} = \frac{q}{c_p}Z\rho^{n-1}\exp\left(\frac{-E_a}{\widetilde{R}T_0\left(1+\frac{T'}{T_0}\right)}\right) \tag{10}$$

and if we expand the quantity $\frac{1}{1+\frac{T'}{T_0}}$ in the exponential in a series in T' about $T' = 0$ and retain the first two terms, we obtain:

$$\frac{dT'}{dt} = \frac{q}{c_p}Z\rho^{n-1}\exp\left(\frac{-E_a}{\widetilde{R}T_0}\left(1-\frac{T'}{T_0}\right)\right)$$

$$= \frac{q}{c_p}Z\rho^{n-1}\exp\left(\frac{-E_a}{\widetilde{R}T_0}\right)\exp\left(\frac{E_a}{\widetilde{R}T_0^2}T'\right) \ . \tag{11}$$

If we now define a new variable ϕ such that

$$\phi = \frac{E_a}{\widetilde{R}T_0^2}T' \tag{12}$$

and

$$\frac{d\phi}{dt} = \frac{E_a}{\widetilde{R}T_0^2}\frac{dT'}{dt} \tag{13}$$

then we can write

$$\frac{d\phi}{dt} = \left(\frac{q}{c_p}Z\rho^{n-1}\frac{E_a}{\widetilde{R}T_0^2}\exp\left(\frac{-E_a}{\widetilde{R}T_0}\right)\right)\exp\left(\phi\right) = \left(\frac{1}{\tau_i}\right)\exp\left(\phi\right) \tag{14}$$

where

$$\tau_i = \frac{c_p}{q}\frac{\widetilde{R}T_0^2}{E_a}\rho^{-n+1}\frac{1}{Z}\exp\left(\frac{E_a}{\widetilde{R}T_0}\right) \tag{15}$$

is called the *explosion time*. We then differentiate Equation 15 with respect to the density ρ while keeping T_0 constant and simplify:

$$\begin{aligned}
\left(\frac{\partial\tau_i}{\partial\rho}\right)_{T_0} &= \left(\frac{c_p}{q}\frac{\widetilde{R}T_0^2}{E_a}\right)(-n+1)\rho^{-n}\frac{1}{Z}\exp\left(\frac{E_a}{\widetilde{R}T_0}\right) \\
&= \left\{\frac{c_p}{q}\frac{\widetilde{R}T_0^2}{E_a}\rho^{-n+1}\frac{1}{Z}\exp\left(\frac{E_a}{\widetilde{R}T_0}\right)\right\}\frac{(-n+1)}{\rho} \\
&= \frac{\tau_i}{\rho}(-n+1)\ .
\end{aligned} \tag{16}$$

From Equation 16 we obtain an expression for the effective reaction order:

$$n = -\frac{\rho}{\tau_i}\left(\frac{\partial\tau_i}{\partial\rho}\right)_{T_0} + 1\ . \tag{17}$$

The computation to apply this method to calculate n proceeds as follows:

1. We first choose a composition and set the pressure to 1 bar and the temperature to the initial temperature T_0. The density, determined by the pressure and temperature through the ideal gas law, is stored in the variable ρ_0. We then use Cantera to compute a constant pressure explosion and a plot of temperature versus time.

2. The explosion time τ_i is approximated as the time to the maximum temperature gradient.

3. We then choose a slightly larger initial density $\rho_0' = \rho_0 + \rho'$ where $\rho' \ll \rho_0$ and prescribe the same initial temperature T_0 to keep the temperature constant for calculation of the derivative $(\partial\tau_i/\partial\rho)_{T_0}$. We then compute another constant pressure explosion, obtaining a slightly different explosion time τ_i'.

4. The derivative of explosion time with respect to initial density is then approximated as:

$$\left(\frac{\partial\tau_i}{\partial\rho}\right)_{T_0} \approx \frac{\Delta\tau_i}{\Delta\rho} = \frac{\tau_i' - \tau_i}{\rho'}\ . \tag{18}$$

5. The effective reaction order is then calculated from:

$$n \approx -\frac{\rho_0}{\tau_i}\frac{(\tau_i' - \tau_i)}{\rho'} + 1\ . \tag{19}$$

We used the method described above to calculate effective reaction orders for a range of hydrogen-air compositions using several different density intervals, ρ'. The results for $\rho' = 0.05\rho_0$, $0.1\rho_0$, $0.15\rho_0$, and $0.2\rho_0$, shown in Figure 1, are all comparable, while the results for $\rho' = 0.01\rho_0$ are erratic because the density interval is too small to correctly approximate the derivative. Therefore, a density interval in the range of $0.05 - 0.30\rho_0$ is acceptable, and $\rho' = 0.10\rho_0$ was used for all subsequent calculations. Values for the effective reaction order calculated for hydrogen-air mixtures using the constant pressure explosion method (Equation 17) are shown in Figure 2. The constant pressure explosion method gives values for n on the order of 2 for all compositions.
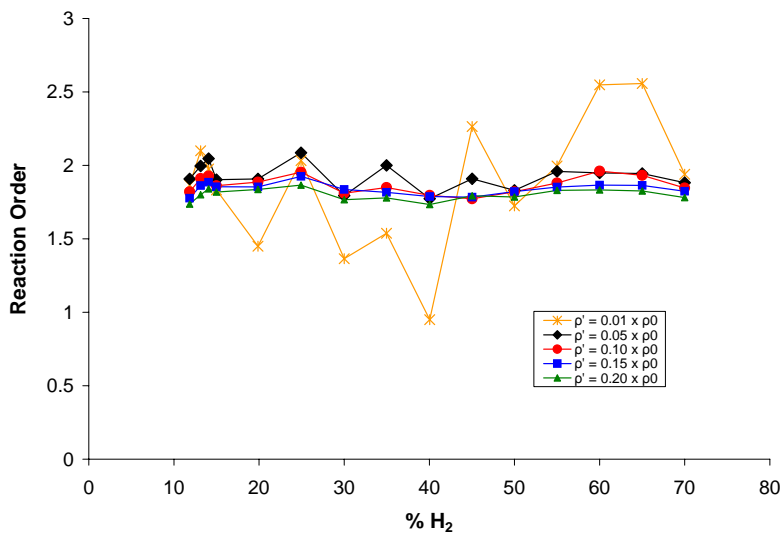
Figure 1: Effective reaction orders for H_2-air mixtures calculated using the constant pressure explosion method (Equation 17) using 5 different density intervals.
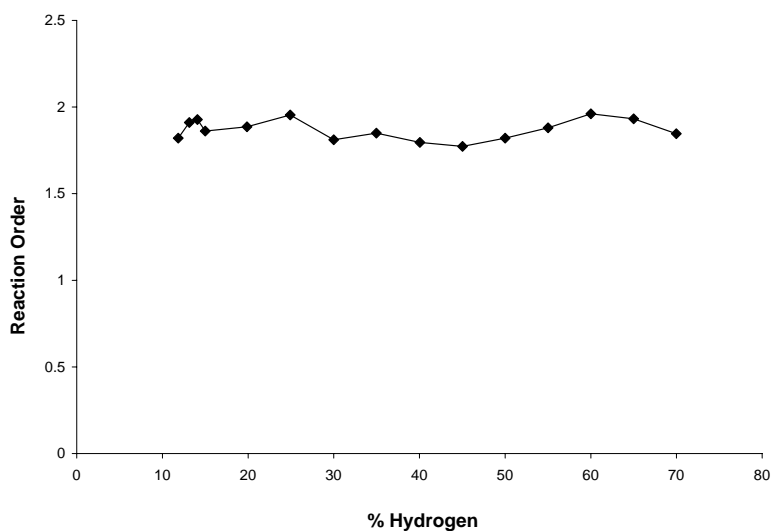
Figure 2: Effective reaction orders for H_2-air mixtures calculated using the constant pressure explosion method (Equation 17).

2.2 Estimating Effective Activation Energy

Applying the ideal gas law to rewrite the density in Equation 15 in terms of pressure and temperature gives

$$\tau_i = \frac{c_p}{q} \frac{\widetilde{R} T_0^2}{E_a} \left(\frac{p}{RT_0} \right)^{-n+1} \frac{1}{Z} \exp \left(\frac{E_a}{\widetilde{R} T_0} \right)$$

$$= \frac{c_p}{q} \frac{\widetilde{R} T_0^{n+1}}{E_a} \left(\frac{p}{R} \right)^{-n+1} \frac{1}{Z} \exp \left(\frac{E_a}{\widetilde{R} T_0} \right) \ . \tag{20}$$

We then differentiate Equation 20 with respect to the temperature T_0 while keeping pressure constant and simplify:

$$\left(\frac{\partial \tau_i}{\partial T_0} \right)_p = \frac{c_p}{q} \frac{\widetilde{R} T_0^{n+1}}{E_a} \left(\frac{p}{R} \right)^{-n+1} \frac{1}{Z} \left(-\frac{E_a}{\widetilde{R} T_0^2} \right) \exp \left(\frac{E_a}{\widetilde{R} T_0} \right)$$

$$+ \frac{c_p}{q} (n+1) \frac{\widetilde{R} T_0^{n}}{E_a} \left(\frac{p}{R} \right)^{-n+1} \frac{1}{Z} \exp \left(\frac{E_a}{\widetilde{R} T_0} \right)$$

$$= \left\{ \frac{c_p}{q} \frac{\widetilde{R} T_0^{n+1}}{E_a} \left(\frac{p}{R} \right)^{-n+1} \frac{1}{Z} \exp \left(\frac{E_a}{\widetilde{R} T_0} \right) \right\} \left(-\frac{E_a}{\widetilde{R} T_0^2} \right)$$

$$+ \left\{ \frac{c_p}{q} \frac{\widetilde{R} T_0^{n+1}}{E_a} \left(\frac{p}{R} \right)^{-n+1} \frac{1}{Z} \exp \left(\frac{E_a}{\widetilde{R} T_0} \right) \right\} \frac{(n+1)}{T_0}$$

$$= \left(-\frac{E_a}{\widetilde{R} T_0} \right) \frac{\tau_i}{T_0} + (n+1) \frac{\tau_i}{T_0} \ . \tag{21}$$

Equation 21 can then be solved for the activation energy E_a:

$$E_a = \widetilde{R} T_0 \left(-\frac{T_0}{\tau_i} \left(\frac{\partial \tau_i}{\partial T_0} \right)_p + (n+1) \right) \ . \tag{22}$$

The computation to apply this method to calculate E_a proceeds as follows:

1. We first choose a composition and set the pressure to 1 bar and the temperature to the initial temperature T_0. We then use Cantera to compute a constant pressure explosion and a plot of temperature versus time.

2. The explosion time τ_i is approximated as the time to the maximum temperature gradient.

3. We then choose a slightly larger initial temperature $T_0' = T_0 + T'$ where $T' \ll T_0$ (in our calculations we used $T' = 30$ K) and set the pressure to 1 bar to keep the pressure constant for calculation of the derivative $(\partial \tau_i / \partial T_0)_p$. We then compute another constant pressure volume explosion, obtaining a slightly different explosion time τ_i'.

4. The derivative of explosion time with respect to initial temperature is then approximated as:

$$\left(\frac{\partial \tau_i}{\partial T_0} \right)_p \approx \frac{\Delta \tau_i}{\Delta T_0} = \frac{\tau_i' - \tau_i}{T'} \ . \tag{23}$$

5. The activation energy is then calculated from:

$$E_a \approx \widetilde{R} T_0 \left(-\frac{T_0}{\tau_i} \frac{(\tau_i' - \tau_i)}{T'} + (n+1) \right) \tag{24}$$

where the reaction order n is the value calculated from Equation 17.

Figure 3 shows Zeldovich numbers and corresponding effective activation energies for hydrogen-air mixtures calculated using the constant pressure explosion method (Equation 22) with the reaction order values shown in Figure 2.

11
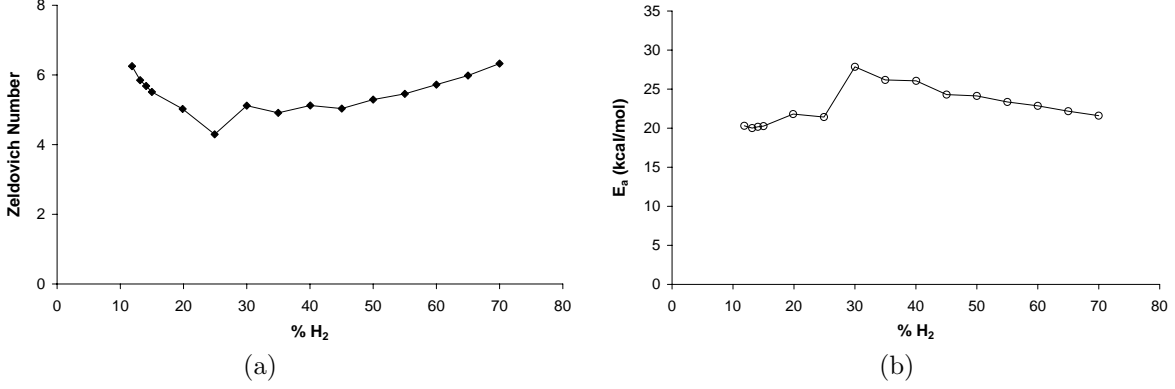
Figure 3: Zeldovich numbers (a) and corresponding effective activation energies (b) calculated using the constant pressure explosion method (Equation 22) with reaction orders obtained from the constant pressure explosion method (Equation 17).

3 Constant Pressure Explosion Method With Constant Volume Initial Conditions

The effective activation energy can also be calculated using constant pressure explosion calculations with constant volume initial conditions. Since mass is conserved, the constant volume condition is imposed by keeping the initial density constant while perturbing the temperature. In this case, because we are neglecting the dependence of the explosion time on initial density, the reaction order does not appear in the expression for the activation energy and so one variable is removed from the calculation.

Differentiating the constant pressure explosion time (Equation 15) with respect to initial temperature T_0 while keeping the density (and hence the volume) constant and simplifying gives:

$$
\begin{aligned}
\left(\frac{\partial \tau_i}{\partial T_0} \right)_\rho &= \frac{c_p}{q} 2 \frac{\widetilde{R} T_0}{E_a} \rho^{-n+1} \frac{1}{Z} \exp \left(\frac{E_a}{\widetilde{R} T_0} \right) \\
&+ \frac{c_p}{q} \frac{\widetilde{R} T_0^2}{E_a} \rho^{-n+1} \frac{1}{Z} \left(-\frac{E_a}{\widetilde{R} T_0^2} \right) \exp \left(\frac{E_a}{\widetilde{R} T_0} \right) \\
&= \left\{ \frac{c_p}{q} \frac{\widetilde{R} T_0^2}{E_a} \rho^{-n+1} \frac{1}{Z} \exp \left(\frac{E_a}{\widetilde{R} T_0} \right) \right\} \left(-\frac{E_a}{\widetilde{R} T_0^2} \right) \\
&+ \left\{ \frac{c_p}{q} \frac{\widetilde{R} T_0^2}{E_a} \rho^{-n+1} \frac{1}{Z} \exp \left(\frac{E_a}{\widetilde{R} T_0} \right) \right\} \frac{2}{T_0} \\
&= \left(-\frac{E_a}{\widetilde{R} T_0} \right) \frac{\tau_i}{T_0} + 2 \frac{\tau_i}{T_0} \ .
\end{aligned}
\tag{25}
$$

We then solve Equation 25 for the effective activation energy E_a:

$$
E_a = \widetilde{R} T_0 \left(-\frac{T_0}{\tau_i} \left(\frac{\partial \tau_i}{\partial T_0} \right)_\rho + 2 \right) \ .
\tag{26}
$$

The computation to apply this method to calculate E_a proceeds as follows:

1. We first choose a composition and set the pressure to 1 bar and the temperature to the initial temperature T_0. The density, determined by the pressure and temperature through the ideal gas law, is stored in the variable ρ_0. We then use Cantera to compute a constant pressure explosion and a plot of temperature versus time.

12

2. The explosion time τ_i is approximated as the time to the maximum temperature gradient.

3. We then choose a slightly larger initial temperature $T_0' = T_0 + T'$ where $T' \ll T_0$ and prescribe the same initial density ρ_0 to keep the density (and volume) constant for calculation of the derivative $(\partial \tau_i / \partial T_0)_\rho$. We then compute another constant pressure explosion, obtaining a slightly different explosion time τ_i'.

4. The derivative of explosion time with respect to initial temperature is then approximated as:

$$\left(\frac{\partial \tau_i}{\partial T_0} \right)_\rho \approx \frac{\Delta \tau_i}{\Delta T_0} = \frac{\tau_i' - \tau_i}{T'} \ . \tag{27}$$

5. The effective activation energy is then calculated from:

$$E_a \approx \widetilde{R} T_0 \left(-\frac{T_0}{\tau_i} \frac{(\tau_i' - \tau_i)}{T'} + 2 \right) \tag{28}$$

Figure 4 shows Zeldovich numbers and effective activation energies for hydrogen-air compositions calculated using the constant pressure explosion method with constant volume initial conditions (Equation 26) with the values calculated using the constant pressure explosion method with reaction order dependence (Equation 22). The two slightly different methods give nearly the same results, with the Zeldovich numbers differing by less than 0.25 and the activation energies differing by less than 1 kcal/mol over the full range of compositions.

Figure 4: Zeldovich numbers (a) and corresponding effective activation energies (b) calculated using the constant pressure explosion method with reaction order dependence (Equation 22) and from the constant pressure explosion method with constant volume initial conditions (Equation 26).

4 Constant Volume Explosion Method

A third method for calculating the effective activation energy is to use constant *volume* explosion calculations instead of constant pressure calculations. Repeating the same derivation presented in Section 2.2 for the constant volume case, i.e., $e =$ constant where e is the internal energy, results in an expression for the constant volume explosion time:

$$\tau_i = \frac{c_v}{q} \frac{\widetilde{R} T_0^2}{E_a} \rho^{-n+1} \frac{1}{Z} \exp \left(\frac{E_a}{\widetilde{R} T_0} \right) \tag{29}$$

. Differentiating the constant volume explosion time with respect to initial temperature T_0 while keeping the density constant gives:

$$\left(\frac{\partial \tau_i}{\partial T_0}\right)_\rho = \frac{c_v}{q} 2 \frac{\widetilde{R} T_0}{E_a} \rho^{-n+1} \frac{1}{Z} \exp\left(\frac{E_a}{\widetilde{R} T_0}\right)$$

$$+ \frac{c_v}{q} \frac{\widetilde{R} T_0^2}{E_a} \rho^{-n+1} \frac{1}{Z} \left(-\frac{E_a}{\widetilde{R} T_0^2}\right) \exp\left(\frac{E_a}{\widetilde{R} T_0}\right)$$

$$= \left\{\frac{c_v}{q} \frac{\widetilde{R} T_0^2}{E_a} \rho^{-n+1} \frac{1}{Z} \exp\left(\frac{E_a}{\widetilde{R} T_0}\right)\right\} \frac{2}{T_0}$$

$$+ \left\{\frac{c_v}{q} \frac{\widetilde{R} T_0^2}{E_a} \rho^{-n+1} \frac{1}{Z} \exp\left(\frac{E_a}{\widetilde{R} T_0}\right)\right\} \frac{1}{T_0} \left(-\frac{E_a}{\widetilde{R} T_0}\right)$$

$$= 2 \frac{\tau_i}{T_0} + \left(-\frac{E_a}{\widetilde{R} T_0}\right) \frac{\tau_i}{T_0} . \tag{30}$$

We can then solve Equation 30 for the effective activation energy:

$$E_a = \widetilde{R} T_0 \left(-\frac{T_0}{\tau_i} \left(\frac{\partial \tau_i}{\partial T_0}\right)_\rho + 2\right) \tag{31}$$

which is identical to Equation 26 except in this method the explosion time is found from a constant volume explosion instead of a constant pressure explosion.

The computation to apply this method to calculate E_a proceeds as follows:

1. We first choose a composition and set the pressure to 1 bar and the temperature to the initial temperature T_0. The density, determined by the pressure and temperature through the ideal gas law, is stored in the variable ρ_0. We then use Cantera to compute a constant *volume* explosion and a plot of temperature versus time.

2. The explosion time τ_i is approximated as the time to the maximum temperature gradient.

3. We then choose a slightly larger initial temperature $T_0' = T_0 + T'$ where $T' \ll T_0$ and prescribe the same initial density ρ_0 to keep the density (and volume) constant for calculation of the derivative $(\partial \tau_i / \partial T_0)_\rho$. We then compute another constant volume explosion, obtaining a slightly different explosion time τ_i'.

4. The derivative of explosion time with respect to initial temperature is then approximated as:

$$\left(\frac{\partial \tau_i}{\partial T_0}\right)_\rho \approx \frac{\Delta \tau_i}{\Delta T_0} = \frac{\tau_i' - \tau_i}{T'} . \tag{32}$$

5. The effective activation energy is then calculated from:

$$E_a \approx \widetilde{R} T_0 \left(-\frac{T_0}{\tau_i} \frac{(\tau_i' - \tau_i)}{T'} + 2\right) . \tag{33}$$

Values of the Zeldovich number and effective activation energy calculated using the constant volume explosion method (Equation 31) are plotted in Figure 5 with results from the constant pressure explosion methods with reaction order dependence (Equation 22) and with constant volume initial conditions (Equation 26). The Zeldovich numbers calculated using the constant volume explosion approach are smaller than the values calculated using the constant pressure explosion methods by about 14% on average due to the higher burned temperature associated with equilibrating a mixture at constant volume versus constant pressure. The effective activation energies calculated using all three methods are comparable, differing by less than 3 kcal/mol over the full range of compositions. These results demonstrate that simple thermal explosion theory provides multiple schemes for extracting consistent and physically reasonable values of both the effective activation energy and effective reaction order with very little computational cost. The complete set of effective reaction orders and activation energies calculated for hydrogen-air mixtures are tabulated in Appendix B.
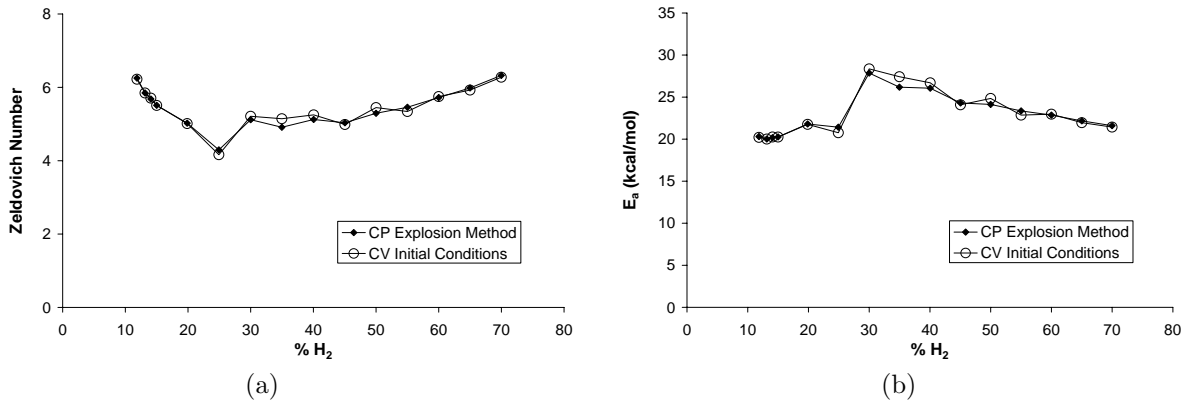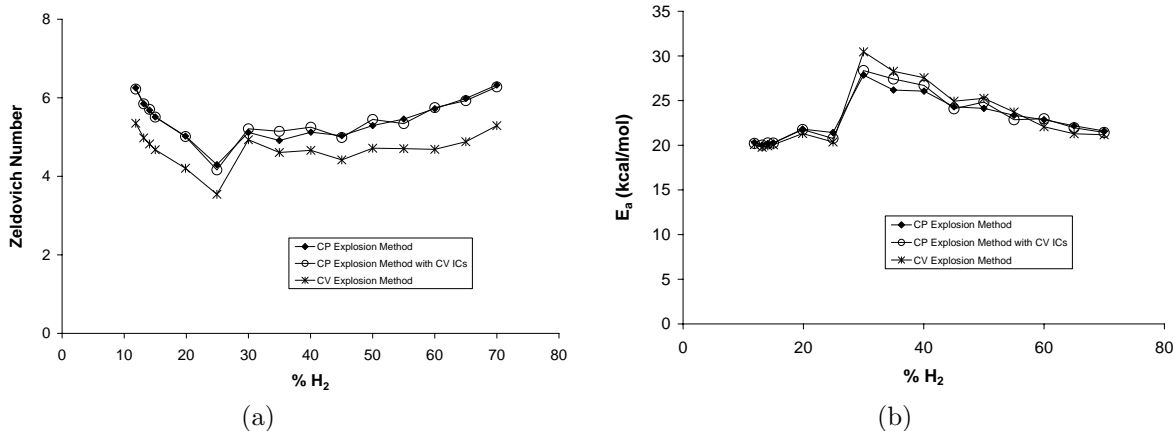
Figure 5: Zeldovich numbers (a) and corresponding effective activation energies (b) calculated using the three different methods: constant pressure explosion method with reaction order dependence (Equation 22), the constant pressure explosion method with constant volume initial conditions (Equation 26), and the constant volume explosion method (Equation 31).

5   Development of One-Step Models for Flame Simulation

5.1   Model Parameters

The first goal of this work was to develop very simple one-step models that would produce flame properties matching those of flames modeled using large multi-step chemical mechanisms. Therefore, to first develop the simplest possible one-step model the following assumptions were used:

1. There are only two species, R (reactant) and P (product).

2. Both species consist of one argon atom, so the molecular weights and transport properties of R and P are the same.

3. The two species have constant specific heat capacity (no temperature dependence). The constant pressure heat capacity of argon at 300 K is used for both R and P (20.785 J/mol·K).

4. The mechanism has one overall reaction $R_1 + \ldots + R_n \xrightarrow{k_f} P_1 + \ldots$ where n is the order of the reaction and k_f is the reaction rate coefficient in the modified Arrhenius form

$$k_f = AT^m \exp\left(-\frac{E_a}{RT}\right) . \tag{34}$$

5. The temperature dependence of the reaction rate is only in the Arrhenius term, i.e. $m = 0$.

These assumptions determine the thermodynamic and transport parameters for the model, leaving four variables: the effective activation energy E_a, effective reaction order n, pre-exponential coefficient A, and the heat released by the reaction q. The effective activation energy and reaction order, E_a and n, are calculated using one of the methods described in Sections 2, 3, or 4 and the pre-exponential coefficient A and the heat release q can be adjusted to produce the desired flame properties. In this work we choose to match the flame speed and flame temperature obtained using a detailed chemical mechanism.

5.2   Implementation of a One-Step Model in the Cantera Flame Code

In this work we use the Python adiabatic 1D flame code included in the Cantera installation and given in Appendix D. The code simulates a freely propagating planar flame, solving for the laminar flame speed

and temperature and species profiles through the flame. Cantera requires a mechanism (.cti) file with thermodynamic and reaction rate data for the species of interest, and it is in this file that we implement the one-step model as described in the previous section.

The structure of the Cantera input file, or .cti file, consists of three sections. In the first section we define an ideal gas consisting of a set of chemical elements, species, and reactions with a chosen transport model and initial state (temperature and pressure). In our one-step model we have one element argon ("Ar") and two species ("R P") listed in this first section of the input file. The second section consists of the species ideal gas thermodynamic data: the specific heat $c_{P_i} = c_{P_i}(T)$, specific enthalpy $h_i = h_i(T)$, and the pressure-independent part of the entropy $s_{oi} = s_{oi}(T)$. The Cantera software uses a piecewise polynomial representation of the specific heat at constant pressure in non-dimensional form

$$\frac{c_{P_i}}{R} = \begin{cases} \sum_{n=0}^{4} a_{ni} T^n & T_{min} \leq T \leq T_{mid} \\ \sum_{n=0}^{4} b_{ni} T^n & T_{mid} \leq T \leq T_{max} \end{cases} . \tag{35}$$

In complex mechanisms, the constants a_{ni} and b_{ni} have to be determined by fitting the polynomial representation to tabular data. However, in our simple one-step model we are using a constant specific heat that is the same for both the reactant (R) and product (P), so the coefficients a_1-a_4 are zero for both species R and P, and only the first coefficient a_0 is nonzero

$$a_{0R} = a_{0P} = \frac{(c_P)_{Ar,300K}}{R} = \frac{20.785 \frac{J}{molK}}{8.314 \frac{J}{molK}} = 2.50 . \tag{36}$$

The enthalpy can be found simply by integrating the specific heat, giving a relationship between the enthalpy and the fifth constant in the thermodynamic data, a_{5i}

$$a_{5i} = \frac{\Delta_f h_i^o}{R_i} - \sum_{n=0}^{4} \frac{a_{ni}}{n+1} (T^o)^{n+1} . \tag{37}$$

In the one-step model, the heat release q is defined as the difference in the enthalpies of the reactants and products

$$q = h_R - h_P \tag{38}$$

so the heat release is related to the constants a_{5i} and a_{0i} as follows:

$$\frac{q}{R} = (a_{5R} - a_{5P}) + (a_{0R} - a_{0P})T^o . \tag{39}$$

In our simple model, $a_{0R} = a_{0P}$ so the heat release is simply $R(a_{5F1} - a_{5F2})$. The last constant, a_{6i} is related to the pressure-independent portion of the entropy, and is left unchanged in our model.

The last section in the input file lists the chemical reactions along with the chemical rate coefficient parameters A, m, and E_a. In the one step model there is only one reaction $R_1 + \ldots + R_n \xrightarrow{k_f} P_1 + \ldots$, and for our model $m = 0$. The one-step parameters q (implemented through the constants a_{5i}), A, and E_a can be changed to produce a flame with the desired properties. An example set of flame profiles generated using a one-step model and profiles generated using detailed chemistry for stoichiometric hydrogen-air are shown in Figure 6. We were able to match the flame speeds and temperatures over a range of compositions for hydrogen-air and propane-air systems. However, we could not match density since we are modeling a complicated multi-species system using a single species so the effects of varying molar mass cannot be simulated correctly; this issue is addressed in a later phase of the work.

6 Two-Species One-Step Model for Hydrogen-Air Systems

We constructed one-step models for hydrogen-air systems using the effective activation energies calculated using the constant pressure explosion method (Equation 22) and listed in Table 2 in Appendix B. The goal
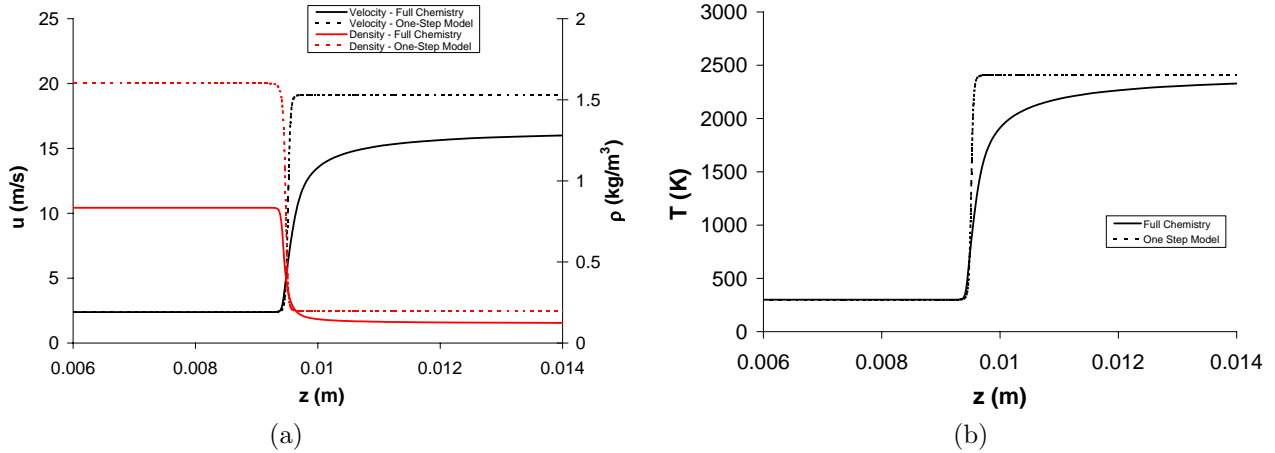
Figure 6: Profiles of the velocity and density (a) and temperature (b) through the flame generated using both the one-step model and full chemistry for stoichiometric hydrogen-air.

was to choose values for the heat release parameter q and the pre-exponential factor A in the one-step model to produce a flame with a flame speed s_L and flame temperature T_b that match the values obtained using detailed chemistry. The heat release is found simply from the increase in temperature:

$$q = c_p \left(T_b - T_u \right) \tag{40}$$

where c_p is the specific heat of the reactant and product in the one-step model, T_u is the initial unburned temperature of the reactant, and T_b is the burned temperature of the product (flame temperature). In our one-step model we use argon to represent both the reactant and the product, so the specific heat c_p used is 20.785 J/mol·K and the initial temperature T_u is 300 K. The flame temperature T_b is found from flame calculations performed using the H_2/O_2 oxidation mechanism published by (Li et al., 2004). The heat release calculated from Equation 40 is incorporated into the Cantera input (.cti) file through the coefficient $(a_5)_P$. We then iterate on A to match the flame speed from the flame calculations using detailed chemistry.

6.1 First Order Reaction

We first constructed one-step models for the first order reaction R $\rightarrow$ P, and the results for the flame speed and flame temperature over a range of hydrogen-air compositions are shown in Figure 7 with the results using detailed chemistry. Using one-step models we were able to match the flame temperature to the result from detailed chemistry to within 1% over the entire range of compositions, from very rich (70% hydrogen) to very lean (12% hydrogen). We were also able to match the flamespeed to within 1% of the detailed chemistry values using one-step models over the entire range of hydrogen concentrations. The one-step model parameters E_a, A, q, and $(a_5)_P$ for the range of hydrogen-air mixtures are tabulated in Appendix E.

We also examined the response of the flame speed and flame temperature to changes in the initial temperature and pressure using the one-step model versus the detailed chemistry behavior for a 30% hydrogen-air (near stoichiometric) mixture. We first considered very small changes in the initial temperature and pressure, 10 K and 0.05 bar respectively. We then calculated the response to small changes in initial temperature by fixing the initial pressure at 1 bar and varying the initial temperature from 290 K to 350 K and computing flamespeed and flame temperature using both the one-step model and detailed chemical mechanism. Similarily, we computed the response to small changes in initial pressure by fixing the initial temperature at 300 K and varying the pressure from 0.8 bar to 1.3 bar. The resulting flamespeed and flame temperature response is shown in Figure 8. For small changes in initial temperature both the flamespeed and flame temperature response produced by the one-step model match the results from detailed chemistry to within 5%. For small changes in initial pressure, the flame temperature response using the one-step model matches the detailed chemistry to within 1%. The flamespeed response to small pressure change using the one-step

17

Figure 7: Flame speeds (a) and flame temperatures (b) calculated using first order one-step models and the Li et al. mechanism (Li et al., 2004) for hydrogen-air compositions.

model, while matching the detailed chemistry to within 11%, is clearly of a different functional form. The flamespeed obtained using detailed chemistry is insensitive to small changes in the initial pressure (near 1 bar), staying nearly constant, while the flamespeed calculated using the one-step model depends on the pressure like $s_L \sim p^{-1/2}$. We see this dependence because in the one-step model we use a first order reaction R → P and from simple flame theory we know that

$$s_L \sim p^{\left(\frac{n-2}{2}\right)} \tag{41}$$

so with $n = 1$ we get $s_L \sim p^{-1/2}$. However, we previously calculated that the reaction order is closer to $n = 2$ for stoichiometric hydrogen-air which gives no dependence of flame speed on pressure. This difference in effective reaction order between the one-step model and detailed chemistry calculations explains the notable difference in the flame speed response to changes in initial pressure.

We also calculated the flame speed and flame temperature response to large changes in initial temperature and pressure, extending the temperature to 800 K and pressure to 8 bar. The results from the one-step model and detailed chemistry are shown in Figure 9. The flame speed calculated using the one-step model is about 5 to 15% larger than the flamespeed found using detailed chemistry as we increase the initial temperature from 350 K to 800 K. The flame temperature from the one-step model is 3 to 11% larger than the detailed chemistry flame temperature, an effect that can be explained by examining the enthalpy. Across a flame the enthalpy is approximately constant, i.e.,

$$h_{Reactants}(T_{Reactants}) = h_{Products}(T_{Products}) \tag{42}$$

where

$$h(T) = \sum_{i=1}^{K} Y_i h_i(T) = \sum_{i=1}^{K} \left(Y_i h_{0,i} + Y_i \int_{T_0}^{T} c_{p,i}(T') \ dT' \right) \tag{43}$$

where Y_i is the mass fraction of species i and K is the total number of species. The flame temperature, or $T_{Products}$, is determined by the enthalpy balance, Equation 42. In our one-step model, the change in species mass fraction is simply $Y_{Reactant} \rightarrow 0$ and $Y_{Product} \rightarrow 1$ and the specific heats $c_{p,Reactant}$ and $c_{p,Product}$ are equal and constant. In flame calculations using detailed chemistry, however, there are many more species so the change in enthalpy due to the change in mass fractions, $\sum Y_i h_{0,i}$ is different than in the one-step chemistry case. Additionally, in the detailed chemistry case the specific heats of all the species increase with temperature, resulting in a lower flame temperature than the in one-step calculation where the specific heat is constant. We match the flame temperature at an initial temperature 300 K by choosing the heat release parameter in the one-step model, but the differences in the enthalpy change result in a different dependence

18

(a)

(b)

(c)

(d)
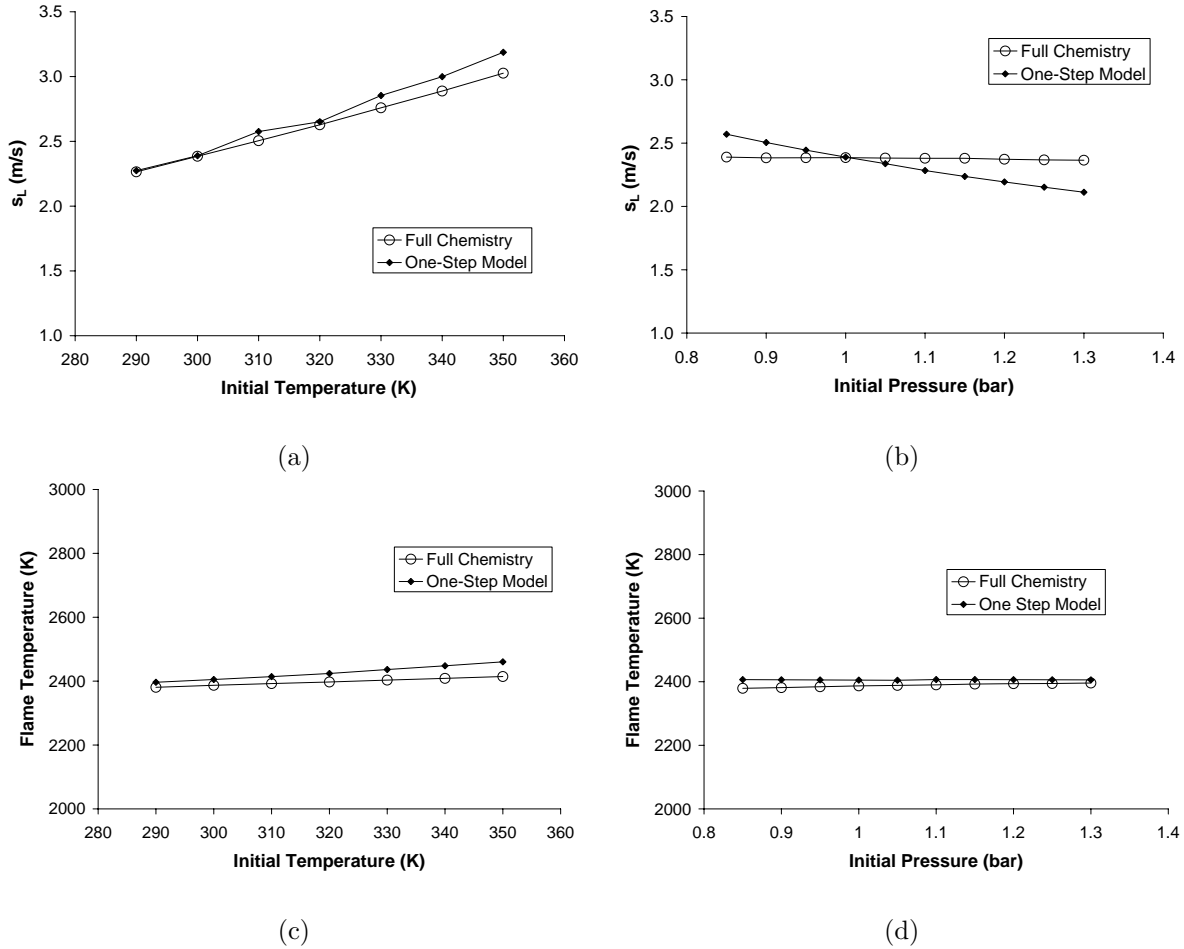
Figure 8: Flame speed response to small changes in initial temperature (a) and pressure (b) and flame temperature response to initial temperature (c) and pressure (d) calculated using first order one-step models and detailed chemistry (Li et al., 2004) for 30% hydrogen-air.

of the flame temperature on initial temperature between the two models and a higher flame temperature for the one-step case. We can change the slope of the flame temperature curve in the one-step case to better match the detailed chemistry curve by increasing the specific heat of the product. However, this change adds additional complexity to the one-step model and may not be necessary as we are able to match the flame temperature response to within 11% with the current model.

As expected, the flame temperature has little response to initial pressure, only increasing by about 50 K from 1 bar to 8 bar, and the one-step model matches the detailed chemistry to within 1% over the entire range of pressure. The difference in the flamespeed response to initial pressure calculated using the one-step model and detailed chemistry is more evident as the initial pressure increases. The one-step model flamespeed clearly exhibits the dependence on pressure $s_L \sim p^{-1/2}$, deviating from the detailed chemistry flamespeed by up to 50%. The detailed chemistry flamespeed does notably decrease with increasing pressure, a trend that is due to the increasing rate of the 3-body reaction $H + O_2 + M \rightarrow HO_2 + M$ slowing the energy release rate. This pressure dependence is a separate effect from the reaction order effect in Equation 41 and therefore cannot be reproduced with a simple one-step chemistry model.

19
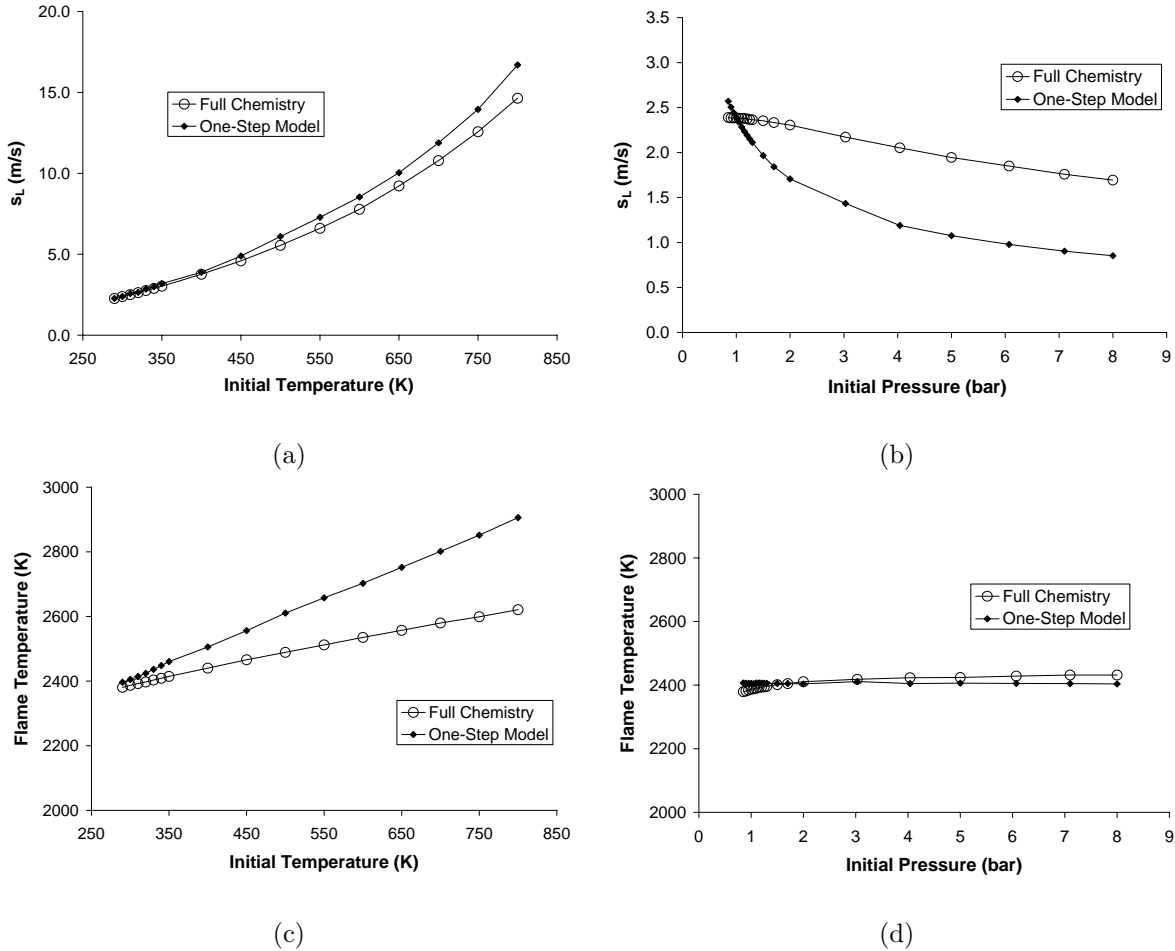
Figure 9: Flame speed response to large changes in initial temperature (a) and pressure (b) and flame temperature response to initial temperature (c) and pressure (d) calculated using first order one-step models and detailed chemistry (Li et al., 2004) for 30% hydrogen-air.

6.2 Second Order Reaction

To improve the flame speed response to pressure in the one-step model, we implemented the second order reaction R + R → P + P in our one-step Cantera input file, prescribing a reaction order $n = 2$ that is closer to the effective reaction orders we previously calculated. We then constructed one-step models for the entire range of hydrogen-air compositions using a second order reaction with the same effective activation energies and heat release parameters found for the first order ($n = 1$) one-step models. Because of the larger reaction order the pre-exponential factor must increase, so we iterated on the pre-exponential factor A until the one-step model flame speed matched the detailed chemistry flame speed. Using the second order one-step models we were once again able to match the flame temperature and flame speed to the detailed chemistry results to within 1% over the entire range of compositions, as shown in Figure 10. The one-step model parameters for the second order ($n = 2$) reaction are tabulated in Appendix E.

As in Section 6.1, we examined the response of the flame speed and flame temperature to changes in the initial temperature and pressure using the new second order one-step model compared with the detailed chemistry behavior for a 30% hydrogen-air mixture. We first considered small changes in initial temperature and pressure by varying the temperature from 290 K to 350 K by 10K (with the pressure fixed at 1 bar) and the pressure from 0.8 bar to 1.3 bar by 0.05 bar (with the temperature fixed at 300 K). The resulting flamespeed and flame temperature response is shown in Figure 11. Once again, for small changes
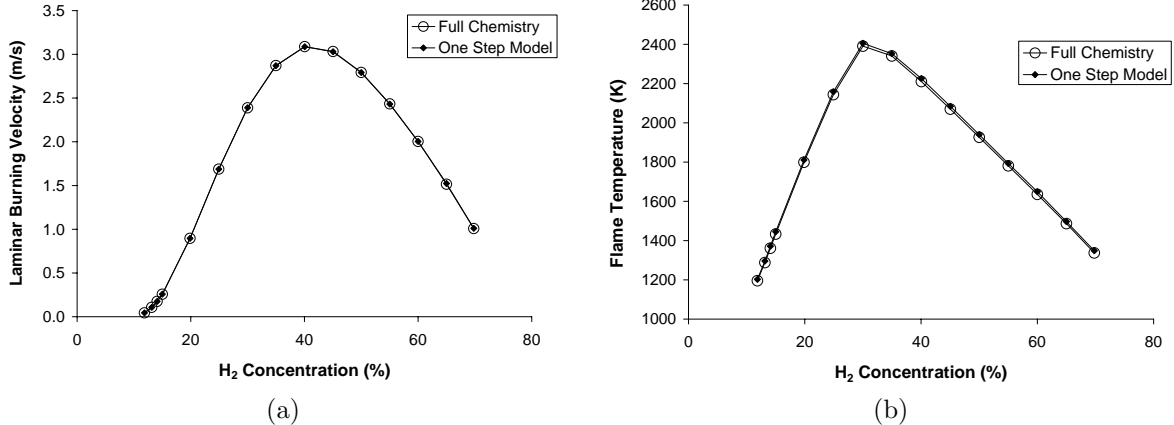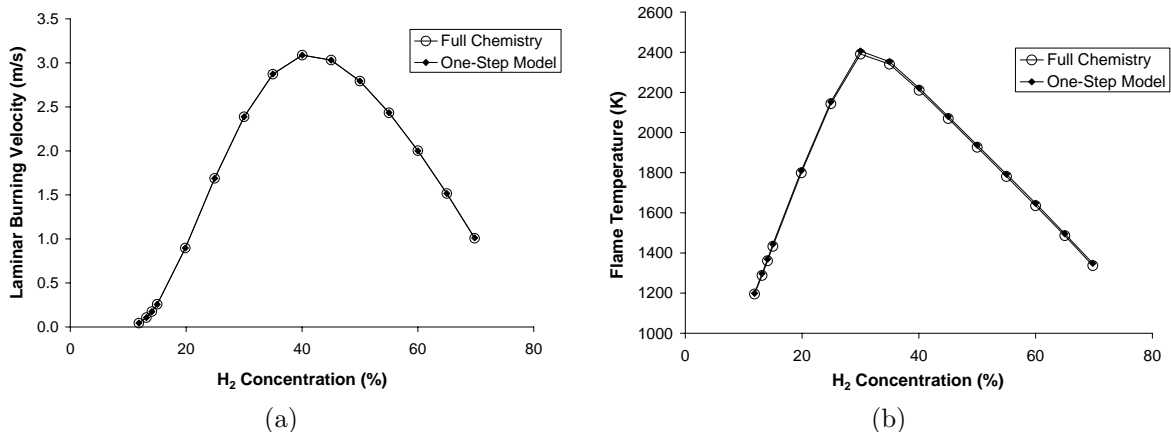
Figure 10: Flame speeds (a) and flame temperatures (b) calculated using second order one-step models and the Li et al. mechanism (Li et al., 2004) for hydrogen-air compositions.

in initial temperature both the flamespeed and flame temperature response produced by the one-step model are in good agreement with the detailed chemistry, with the flamespeed and temperature matching the detailed chemistry values to within 6% and 2%, respectively. Also, we once again match the one-step flame temperature response to small pressure change to within 1%. Most notable is the change in the flamespeed response to small pressure changes using a second order one-step model. The agreement with the detailed chemistry behavior is greatly improved and the one-step model values match the detailed chemistry results to within 2.5%.

As in Section 6.1 we also calculated the flame speed and flame temperature response to large changes in initial temperature and pressure, and the results are shown in Figure 12. Like with the first order one-step model, the one-step flame speed is about 5 to 15% larger than the detailed chemistry flamespeed as we increase the initial temperature from 350 K to 550 K. For initial temperatures above 550 K the difference between the one-step and detailed chemistry flamespeeds increases up to 33% until the one-step flamespeed increases dramatically to 27 m/s and 76 m/s at initial temperatures of 750 K and 800 K, respectively. This phenomenon of rapidly increasing flamespeed is a common issue with modelling high speed combustion waves (see (Singh et al., 2003) for more details). As the flamespeed increases the effects of diffusion decrease and the pre-heat region of diffusion-convection balance disappears, resulting in a predominant balance between convection and reaction. In this situation the solution is no longer a typical flame, but rather the "fast flame" or "convected explosion" solution. The flame temperature from the one-step model is 2 to 10% larger than the detailed chemistry flame temperature due to the same reasons as described in Section 6.1 for the first order one-step model.

Once again, the flame temperature only increases by about 50 K for initial pressure increasing from 1 bar to 8 bar, and the one-step model matches the detailed chemistry to within 1% over the entire range of pressure. While increasing the effective reaction order in the one-step model from $n = 1$ to $n = 2$ gives better agreement between the flamespeeds calculated using the one-step model and detailed chemistry, there is still a large (up to 40%) difference for high initial pressures due to the decrease in the detailed chemistry flamespeed. As described before, this flamespeed decrease is due to the increasing rate of the 3-body reaction $H + O_2 + M \rightarrow HO_2 + M$ as the initial pressure increases. Figure 13 shows the flamespeed versus initial pressure calculated using detailed chemistry, the first order one-step model, and the second order one-step model for the 30% hydrogen case. Also shown is the flamespeed calculated using the effective reaction order $n = 1.8$ (found previously using the constant pressure explosion method, Equation 17) and the pressure dependence

$$s_L \sim p^{\left(\frac{n-2}{2}\right)} = p^{-0.1} \tag{44}$$

where the flame speed with $n = 1.8$ was scaled to match the detailed chemistry flame speed at 1 bar. The flame speed versus pressure calculated using detailed chemistry lies between the first order one-step model

21

with pressure dependence $s_L \sim p^{-1/2}$ and the second order one-step model with no pressure dependence ($s_L \sim p^0$). The scaled flame speed values generated using $n = 1.8$ match the detailed chemistry results very closely (within 16% over the entire range of pressure), however, fractional reaction orders cannot be used in the one-step model. Therefore, the flamespeed dependence on pressure cannot be properly modelled using one-step chemistry for large changes in initial pressure. The pressure dependence could be improved by using multi-step models, but a second order one-step model is much easier to implement and the flamespeed response to small changes in initial pressure (up to 2 bar) is reasonable, within 5% of the detailed chemistry results.
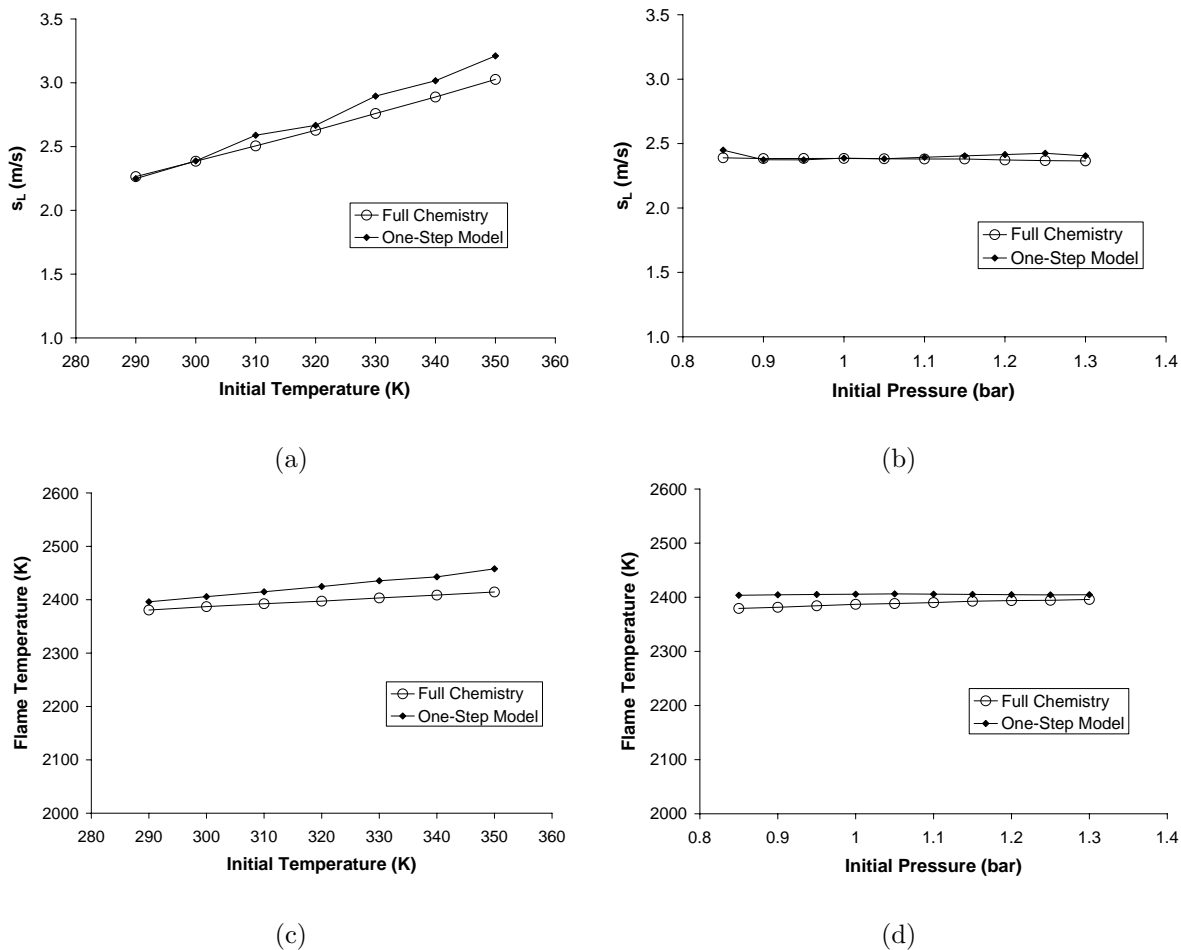
Figure 11: Flame speed response to small changes in initial temperature (a) and pressure (b) and flame temperature response to initial temperature (c) and pressure (d) calculated using second order one-step models and detailed chemistry (Li et al., 2004) for 30% hydrogen-air.

7 Multi-Species One-Step Model: Flame Strain and Extinction

7.1 Strained Flame Calculations

In the first phase of this work, one-step chemistry models were used to accurately simulate the flame speed, flame temperature, and flame response to small changes in the initial pressure and temperature for a range of hydrogen-air mixtures. In these models, we assumed that there were only two species, the reactant (R) and product (P), and that both of these species had the specific heat and transport properties of an argon atom.

(a)

(b)

(c)

(d)
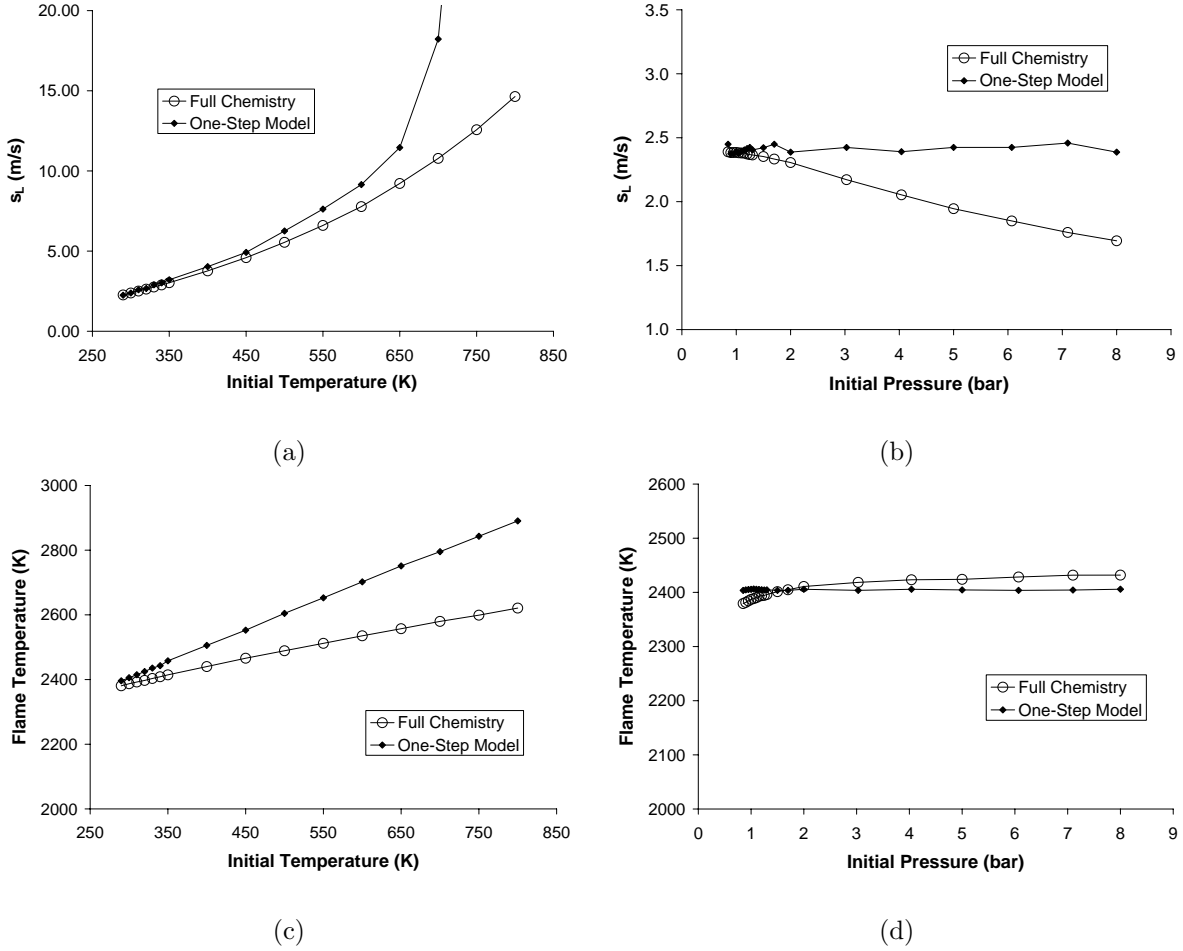
Figure 12: Flame speed response to large changes in initial temperature (a) and pressure (b) and flame temperature response to initial temperature (c) and pressure (d) calculated using second order one-step models and detailed chemistry (Li et al., 2004) for 30% hydrogen-air.

In the second phase of this work, we examined the response of the one-step model flame to turbulence by performing simple strained flame simulations using the Cantera Python script *STFLAME1.py*. The script simulates a 1D flame in a strained flow field generated by an axisymmetric stagnation point, as illustrated in Figure 14. The flame starts out at a burner 6 mm above a non-reacting surface and as the mass flow rate from the burner is increased, the flame moves closer to the surface until it is extinguished. The Python script is given in Appendix G.

An initial grid is defined along the z-axis from $z = 0$ (the burner outlet) to $z = 0.06$ m (the surface) and the code calculates the flow velocity, temperature, and species along the axis using grid refinement. Examples of the calculated velocity and temperature along the z-axis for a 15% hydrogen-air mixture with a mass flow rate $\dot{m} = 2$ kg/m^2·s are given in Figure 15. The slope of the velocity, plotted in Figure 16, provides a measure of the rate of strain in the flowfield, and so the highest rate of change of the velocity is taken as the strain rate, a, i.e.,

$$\left| \frac{du}{dz} \right|_{max} = a \tag{45}$$

Taking the absolute value of the derivative is necessary because the slope of the velocity is negative upstream of the flame. The derivative of the velocity is calculated numerically, and the strain rate is recorded as well as the maximum temperature. The maximum temperature decreases as the mass flow rate, and hence the

23
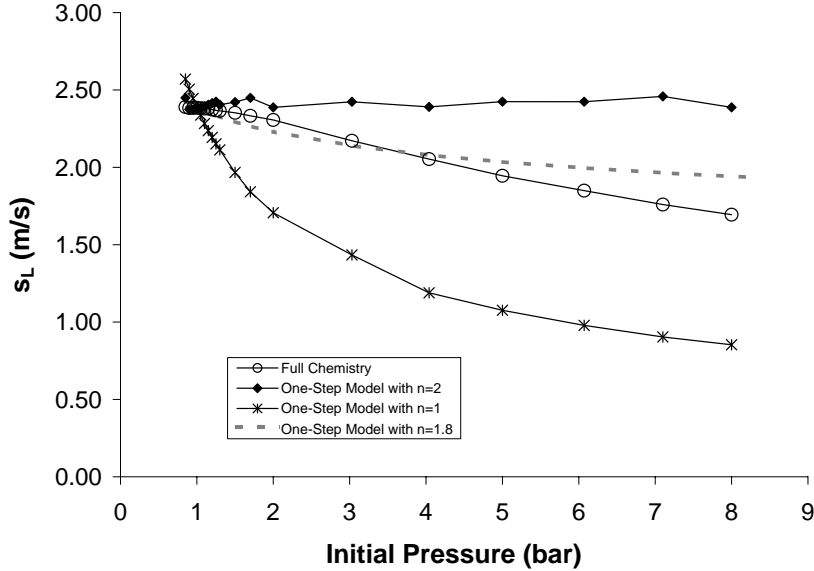
Figure 13: Flame speed response to changes in initial pressure calculated using detailed chemistry (Li et al., 2004), a first order one-step model, and a second order one-step model for 30% hydrogen-air. Also shown (red dashed line) is the predicted one-step model flamespeed with effective reaction order $n = 1.8$ obtained from the constant pressure explosion model (Equation 17).

strain rate, is increased until the flame is extinguished. Plotting the maximum temperature versus the strain rate allows us to study the extinction behavior of strained flames.

7.2 Two-Species One-Step Model

The Cantera code was used to calculate strained flames for a 15% hydrogen-air mixture using both detailed chemistry and a one-step model, and the maximum temperature versus strain rate is plotted in Figure 17. The extinction strate rate with detailed chemistry is approximately 1070 s^{-1}, while the extinction strain rate with the one-step model was nearly 5 times lower, approximately 223 s^{-1}. This large difference is due to the different Lewis numbers in the two cases. The Lewis number of a mixture is defined as the ratio of the thermal diffusivity to the mass diffusivity:

$$Le = \frac{\alpha}{D} = \frac{\kappa/(\rho c_P)}{D} \tag{46}$$

where κ is the thermal conductivity, ρ is the density, c_P is the constant pressure specific heat, and D is the binary diffusion coefficient of the limiting species and the neutral diluent. In the case of the 15% hydrogen-air mixture, since the mixture is lean ($\phi < 0$) the limiting species is hydrogen. For most gases, the Lewis number is close to unity, but for this mixture the Lewis number is less than 1 due to the large mass diffusivity of hydrogen. Using the detailed chemical mechanism, we can calculate the Lewis number for the mixture in Cantera:

$$Le = \frac{\frac{0.0405 \ \frac{J}{s \cdot m \cdot K}}{\left(0.9953 \ \frac{kg}{m^3}\right)\left(1.1718 \ \text{x} \ 10^3 \ \frac{J}{kg \cdot K}\right)}}{9.24 \ \text{x} \ 10^{-5} \ \frac{m^2}{s}} = 0.38 \ . \tag{47}$$

Therefore for this lean hydrogen mixture the Lewis number is significantly less than 1, allowing for a much higher extinction strain rate than typical gas mixtures. In the one-step model the reactant is treated as an argon atom, so the mass diffusivity is nearly an order of magnitude smaller (1.895 x 10^{-5} m^2/s versus 9.24 x 10^{-5} m^2/s for hydrogen) and thus the Lewis number is close to unity (Le = 1.14 for the one-step model).

24
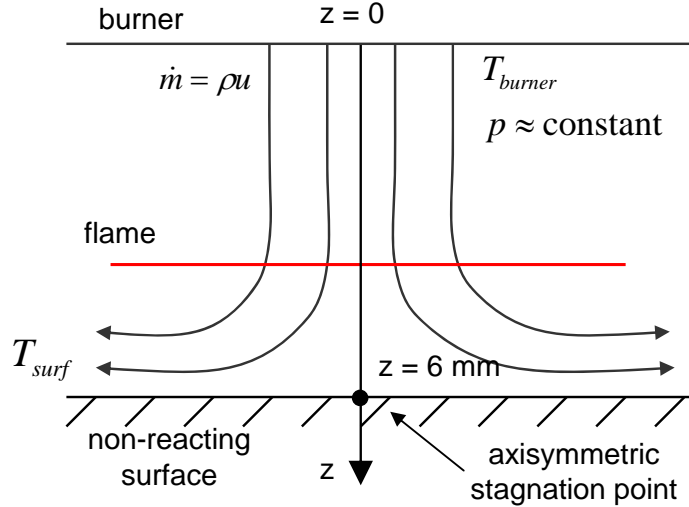
Figure 14: Schematic of axisymmetric stagnation point flow used to study flame strain in the Cantera script *STFLAME1.py.*

Therefore, with the simple two-species (both argon) one-step model much lower extinction strain rates will be observed.

7.3 Four-Species One-Step Model with Realistic Transport Properties

To simulate the straining behavior more accurately, we changed the one-step model in an attempt to match the Lewis number obtained with detailed chemistry. The new one-step model included the four species H_2, O_2, H_2O, and N_2 instead of the two species R and P. The specific heats of H_2, O_2, and H_2O were increased by a factor of approximately 3 to reduce the numerator of the Lewis number; for N_2 the actual thermodynamic coefficients for a nitrogen molecule were used. Also, the actual transport coefficients for all 4 species were used so that the mass diffusivity matched that in the detailed chemistry case. The one-step reaction was changed from R + R $\rightarrow$ P + P to the model reaction $H_2 + \frac{1}{2}O_2 \rightarrow H_2O$ with effective parameters $E_a = 20.263$ kcal/mol and $A = 2.85 \times 10^{14}$ s^{-1}. Finally, since all the actual species are included, the initial composition is the same as in the detailed chemistry case: $0.42H_2 + 0.5O_2 + 1.88N_2$. After these

(a)

(b)
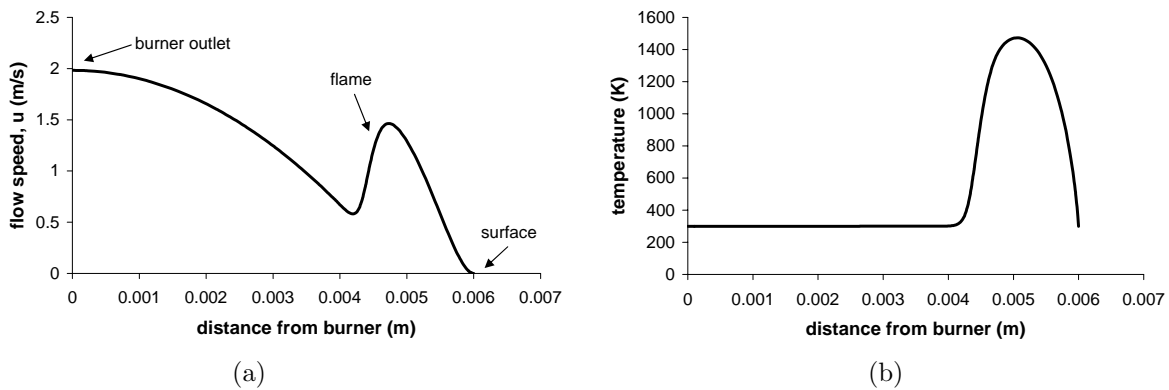
Figure 15: Flow velocity (a) and temperature (b) between the burner and the surface, calculated by the Cantera code. The flame location is indicated by the increase in velocity and temperature.

25
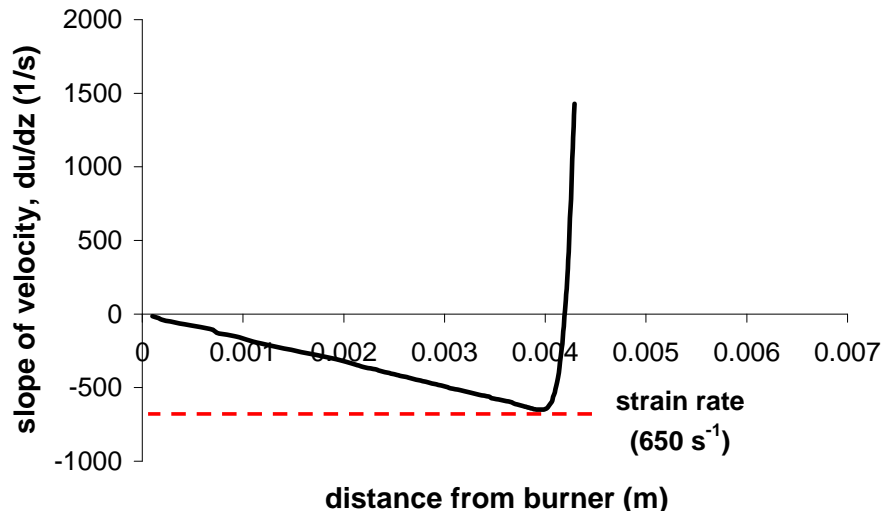
Figure 16: Derivative of the flow velocity along the z-axis, with the strain rate indicated.

changes were implemented, the Lewis number of the mixture obtained with the new one-step model was 0.42, much closer to the actual Lewis number of 0.38. The parameters for the first one-step model, new 4-species one-step model, and the detailed chemistry model are summarized in Table 1 and the Cantera input file for the 4-species one-step model is given in Appendix H.

Table 1: Comparison of parameters in the Lewis number for two one-step models and the detailed chemistry.

	2-Species One-Step Model	4-Species One-Step Model	Detailed Chemistry
Reaction	R + R → P + P	"$H_2 + \frac{1}{2}O_2 \rightarrow H_2O$"	
ρ	1.601 kg/m^3	0.995 kg/m^3	0.995 kg/m^3
c_P	520 J/kg·K	1662 J/kg·K	1171 J/kg·K
κ	0.0181 W/m·K	0.0507 W/m·K	0.0405 W/m·K
D_{H_2}	1.89 x 10^{-5} m^2/s	9.24 x 10^{-5} m^2/s	9.24 x 10^{-5} m^2/s
Le	1.14	0.42	0.38

As before, the effective activation energy was calculated using the constant pressure explosion method (Section 2) and the reaction is second order since $n \approx 2$. The heat release was determined to match the flame temperature, and the pre-exponential factor A was adjusted to match the flame speed. In addition to matching the flame temperature and speed, the one-step model now also accurately simulates the density because it uses the correct molecular weights and initial composition. Strained flame computations for the 15% hydrogen-air mixture were performed again using the new 4-species one-step model, and the maximum temperature versus strain rate is plotted in Figure 18 for both one-step models and detailed chemistry. As shown in the plot, with the 4-species one-step model we were able to match the extinction strain rate obtained with detailed chemistry, $a_{ext} = 1070$ s^{-1}. Therefore, flames modeled with the 4-species model will more closely simulate flame front response to turbulence than flames calculated using the initial 2-species one-step model.
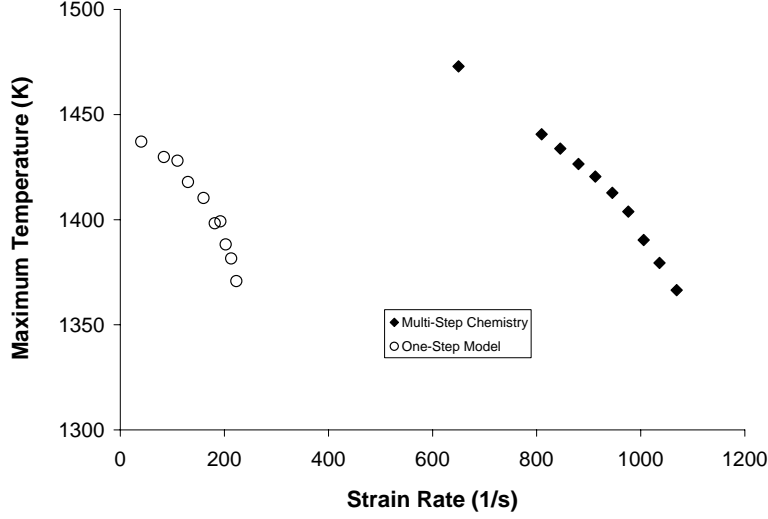
Figure 17: Maximum temperature versus strain rate near extinction for a 15% hydrogen-air mixture.

8 Using One-Step Chemistry Models in Multidimensional Reacting Flow Simulations

8.1 Implementing One-Step Models in AMROC

One-step chemistry models for hydrogen in air were implemented in the fluid dynamics code AMROC (Adaptive Mesh Refinement in Object-Oriented C++) developed by R. Deiterding (Deiterding, 2003). The adaptive mesh refinement (AMR) algorithm of AMROC is especially tailored for time-explicit finite volume schemes of hyperbolic conservation laws. In collaboration with R. Deiterding we first began work in AMROC with the 2D reactive Euler equations solver, then included viscosity and heat transfer conduction in the model. More information on the software can be found on the user group website http://www.cacr.caltech.edu/asc/wiki/bin/view/Amroc/WebHome.

The 4-species one-step model with accurate transport properties for a 15% hydrogen-air mixture was implemented in AMROC, and temperature-dependent transport properties were used like in Cantera. The Sutherland law is used for the heat conductivity and viscosity

$$\mu = \mu_{ref} \left(\frac{T}{T_{ref}} \right)^{\frac{3}{2}} \frac{T_{ref} + s_\mu}{T + s_\mu} \tag{48}$$

$$k = k_{ref} \left(\frac{T}{T_{ref}} \right)^{\frac{3}{2}} \frac{T_{ref} + s_k}{T + s_k} \tag{49}$$

and an empirical equation is used for the mass diffusivity

$$D = D_{ref} \left(\frac{T}{T_{ref}} \right)^{1.71} . \tag{50}$$

The parameters s_μ, s_k, and exponent for the mass diffusivity equation (1.71) were chosen to match the temperature dependence in Cantera; the mass diffusivity, heat conductivity, and viscosity matched the values from Cantera within 6% over the temperature range 300 to 2500 K. The initial condition was a 6th order interpolation of the Cantera solution for the flame profile, and after the errors dissipated the AMROC simulation converged to a steady solution. The profiles of the velocity and temperature across the flame from AMROC and Cantera are compared in Figure 19. The flame profiles computed in AMROC agree with those calculated with Cantera to within 7% for the velocity and 1% for the temperature. The simple simulations indicated that the one-step model was correctly implemented in the AMROC software.

27
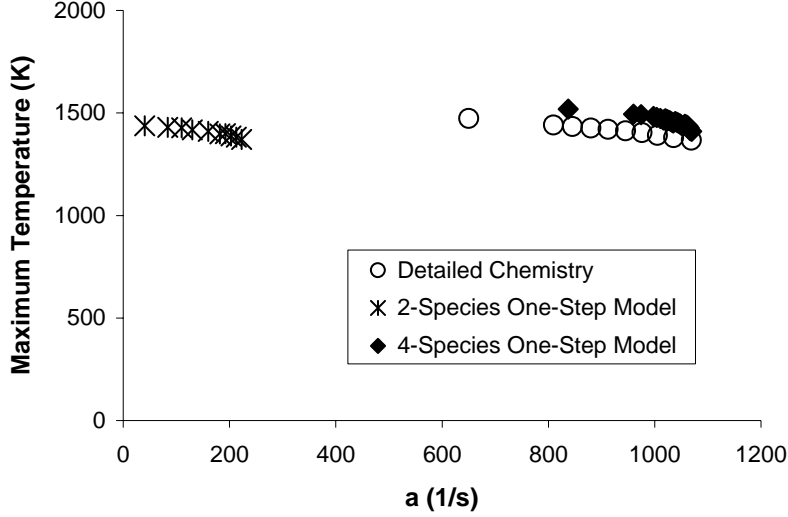
Figure 18: Maximum temperature versus strain rate near extinction for a 15% hydrogen-air mixture using detailed chemistry, the 2-species one-step model with Le = 1.14, and the 4-species one-step model with Le = 0.42.

8.2 Spark Discharge and Ignition Simulations

8.2.1 Spark Discharge in Non-Reactive Gas

We first performed computations in AMROC to simulate the fluid dynamics following a spark discharge from a conical electrode in a non-reactive perfect gas (nitrogen). These computations provide insight into the complicated flow field that evolves after the passing of the shock wave generated by the sudden deposition of energy by the spark discharge. The computational domain is depicted in Figure 20(a) and the initial pressure field in the simulation is shown in Figure 20(b). We assume two planes of symmetry, requiring that the y (radial) and x (axial) velocities be symmetric and therefore model a cylindrical quarter of the whole domain. For the initial conditions, we assume that the spark creates a thin cylindrical channel of gas at extremely elevated pressure and temperature, i.e.,

$$\frac{p_{spark}}{p_{\infty}} = \frac{\rho_{\infty}}{\rho_{spark}} = 10^2 \tag{51}$$

$$\frac{T_{spark}}{T_{\infty}} = 10^4 \; . \tag{52}$$

The pressurized gas channel forms in the gap between two conical electrodes. This is an enormous simplification because we do not attempt to model the spark discharge itself, but it is a starting point for studying the overall problem of flame initiation. The Ghost Fluid Method (GRM) was used to model the solid electrode boundary for both the inviscid and viscous case, and the boundaries were modeled as adiabatic. The refinement criteria are defined so that the physics of each length scale in the problem is captured. The gradients of the density, radial and axial velocities, and energy are used for the convective, viscous, and conductive length scales, respectively. When a gradient across two cells becomes larger than a defined tolerance, a refinement level is added.

We solved the Navier-Stokes equations with heat and mass diffusion with three levels of refinement using 32 processors, with simulation time on the order of one day. Figure 21 shows the pressure field at early times resulting from the shock wave, which is cylindrical in nature near the vertical plane of symmetry but spherical in nature near the electrode surface. This shock structure initiates a complicated flow field, visualized by the evolution of the density field in Figure 22. After the shock wave passes, initially the hot kernel of gas expands outward. However, due to the complicated shock structure, the pressure is higher in the center of the kernel, inducing outflow along the electrodes. A vortex forms due to the separation of the flow at the

28
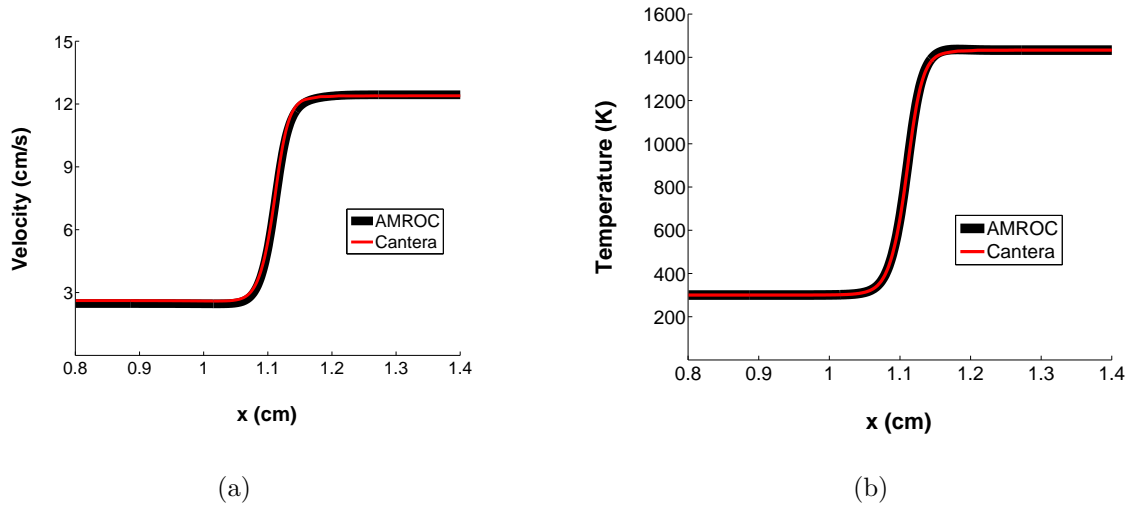
Figure 19: Comparison of the velocity (a) and temperature (b) profiles for a one-dimensional flame simulated in Cantera and AMROC using the improved one-step model with 4 species and realistic transport properties.
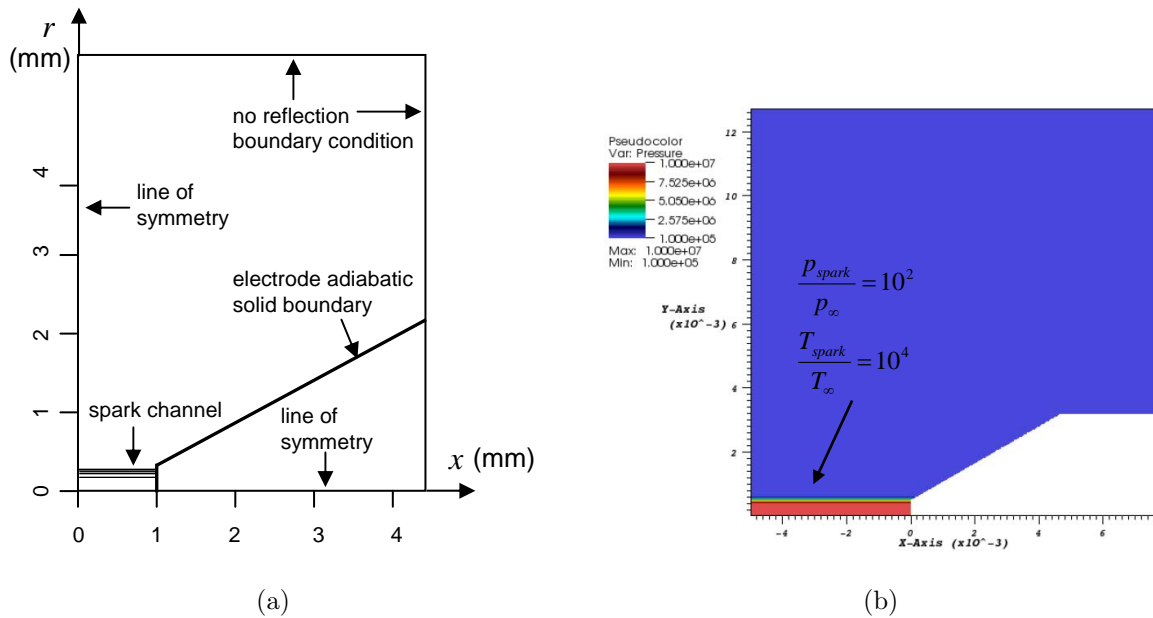
Figure 20: Computational domain (a) and initial pressure field (b) for the spark discharge and ignition simulations.

electrode, which then induces flow inward toward the center of the kernel. The vortex is convected towards the center of the channel and then up and out of the channel, trapping a kernel of hot gas. In addition, a mixing region forms near the end of the channel, mixing hot products with cold reactants. The flow field and the effect of geometry is discussed further in (Bane and Shepherd, 2010).

29
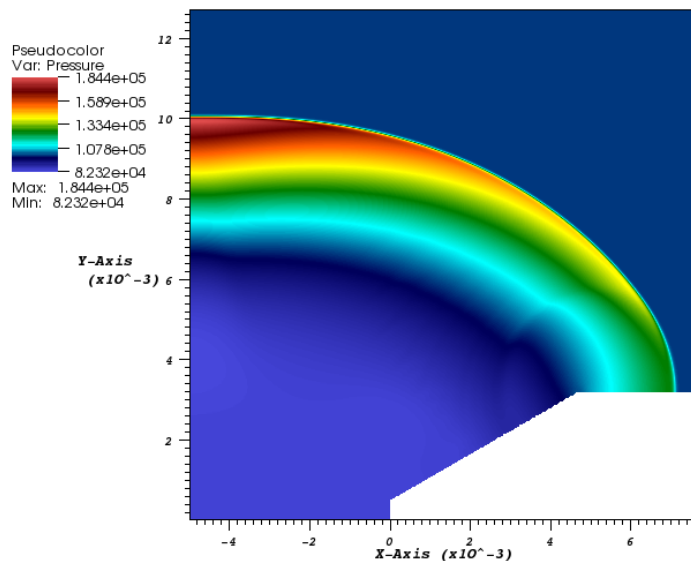
Figure 21: Pressure field resulting from the cylindrical/spherical shock wave in the early stages of the spark discharge simulation.

8.2.2 Spark Ignition in Hydrogen

Preliminary simulations were performed of ignition in a 15% hydrogen-air mixture. The 4-species one-step chemistry model with improved transport properties, presented in Section 7.3, was implemented in AMROC, and the initial conditions described in Section 8.2.1 were used to initiate the flame. The reactive Navier-Stokes equations with heat and mass transport by diffusion were solved with 2 levels of refinement, taking approximately 4 hours on a Linux computer with 32 processors. The evolution of the temperature field during ignition is shown in Figure 23. As expected, the flame front forms on both the hot rising gas kernel generated by the vortex but also in the mixing region. Further ignition simulations are presented in (Bane and Shepherd, 2010).

9 Summary

The objective of this work was to develop methods for extracting physically reasonable parameters for use in one-step chemistry models for flame and ignition simulation. A method based on constant pressure explosion theory was developed to calculate values of the effective reaction order and activation energy for one-step reactions. Constant pressure explosion computations performed using Cantera software were used to estimate effective parameters for a range of hydrogen-air mixtures. The effective activation order was found to be approximately 2, and the effective activation energies ranged between approximately 20 and 28 kcal/mol, a physically reasonable value when compared to the values for the most important chain branching reactions in the detailed chemical mechanism. Two other similar methods for estimating the effective parameters were also developed using constant volume explosions, and the results from the three methods were comparable.

Using the values for n and E_a calculated using the constant pressure explosion method, one-step models were developed for hydrogen-air mixtures and implemented in a Cantera 1D flat flame code. The heat release and reaction rate pre-exponential parameter in the models were chosen such that the flame speed and temperature of the flame calculated with the one-step model matched the values obtained using a detailed chemical mechanism. The first one-step model developed included just two species, the reactant (R) and product (P) and both species consisted of a single argon atom. The response of the flame speed and temperature to changes in the initial pressure and temperature was examined for stoichiometric hydrogen-air. It was found that a one-step model with the second order reaction $R + R \rightarrow P + P$ accurately simulated

30
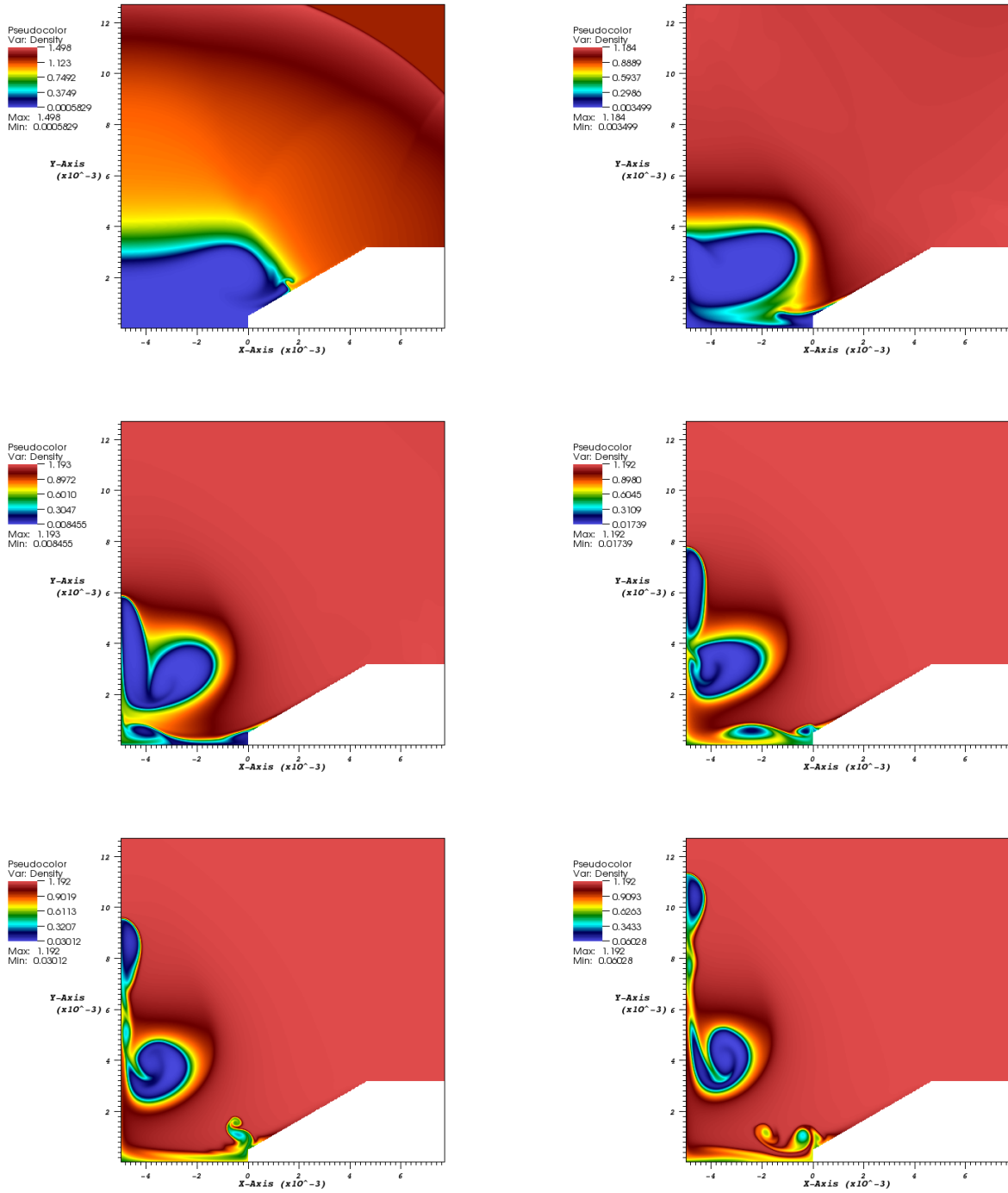
Figure 22: Evolution of the density field for the non-reactive viscous case.

the flame response to small changes in the initial state, while still matching the flame speed and temperature calculated with detailed chemistry. The flame response in a strained flow field was then examined by performing stagnation flame simulations in Cantera using the one-step model for a 15% hydrogen-air mixture. Using the two-species one-step model, the extinction strain rate observed was significantly less than that
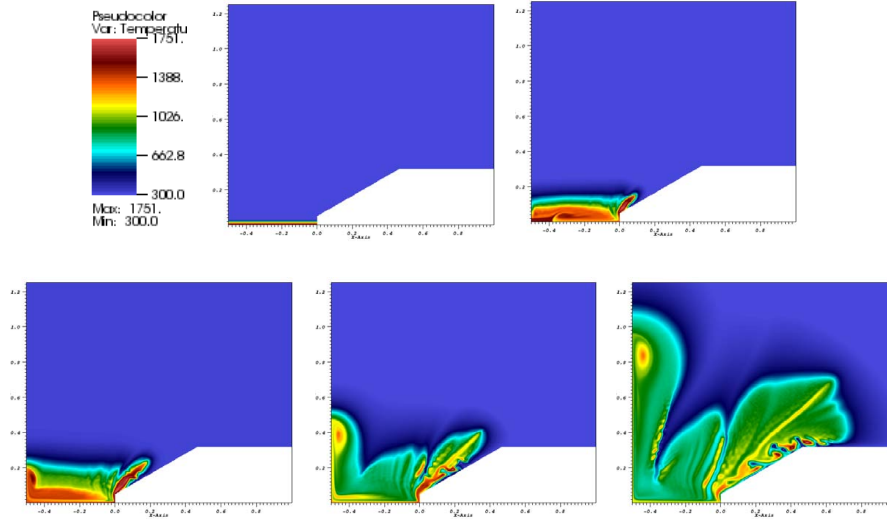
Figure 23: Images of the temperature field from an AMROC simulation of spark ignition of a hydrogen-air mixture.

found using full chemistry. To better simulate the strained behavior, a second one-step model was developed that included four species (H_2, O_2, H_2O, and N_2) and realistic transport parameters. Flames calculated using this new four-species model exhibited that same extinction strain rate as flames calculated using the detailed mechanism.

Finally, the one-step model with four species and realistic transport parameters for 15% hydrogen-air was implemented in the AMROC software to perform ignition simulations. To validate the implementation of the model, a 1D flat flame was simulated in AMROC and the flame profiles were compared with those computed in Cantera. We showed that the 1D flame profiles obtained in AMROC had close agreement with the flame profiles from Cantera, indicating that the one-step model had been successfully implemented in the software. Two-dimensional axisymmetric simulations of spark discharge in a non-reacting gas were performed first to examine the fluid mechanics following the spark discharge. Preliminary simulations of spark discharge and ignition in 15% hydrogen-air were performed by solving the reacting Navier-Stokes equations with heat and mass diffusion and one-step chemistry. Further work on simulating both spark discharge in air and ignition are presented in (Bane and Shepherd, 2010).

References

V. Babrauskas. *Ignition Handbook: Principles and Applications to Fire Safety Engineering, Fire Investigation, Risk Management and Forensic Science.* Fire Science Publishers, Issaquah, WA, 2003.

S. P. M. Bane and J. L. Ziegler J. E. Shepherd. Investigation of the effect of electrode geometry on spark ignition. manuscript in preparation, 2010.

C. R. Bauwens. Research technical memorandum, evaluation of flame properties (fp) program (project no 003025190). Technical report, 2007. FM Global.

R. Deiterding. *Parallel Adaptive Simulation of Multi-dimensional Detonation Structures.* PhD thesis, Brandenburgische Technische Universität Cottbus, 2003.

O. Ekici, O. A. Ezekoye, M. J. Hall, and R. D. Matthews. Thermal and flow fields modeling of fast spark discharges in air. *Journal of Fluids Engineering*, 129:55–65, 2007.

D. Fernández-Galisteo, A. L. Sánchez, A. Li nán, and F. A. Williams. One-step reduced kinetics for lean hydrogen-air deflagration. *Combustion and Flame*, 156:985–996, 2009.

D. Goodwin. Cantera: Object-oriented software for reacting flows, 2005. California Institute of Technology, http://www.cantera.org.

F. F. Grinstein and C. Fureby. Les studies of the flow in a swirl gas combustor. *Proceedings of the Combustion Institute*, 30:1791–1798, 2005.

V. Hamosfakidis, H. G. Im, and D. N. Assanis. A regenerative multiple zone model for hcci combustion. *Combustion and Flame*, 156:928–941, 2009.

M. Kono, K. Niu, T. Tsukamoto, and Y. Ujiie. Mechanism of flame kernel formation produced by short duration sparks. In *Twenty-Second Symposium (International) on Combustion*, pages 1643–1649. The Combustion Institute, Pittsburgh, PA, 1988.

T. Kravchik, E. Sher, and J. B. Heywood. From spark ignition to flame initiation. *Combustion Science and Technology*, 108:1–30, 1995.

J. Li, Z. Zhao, A. Kazakov, and F. L. Dryer. An updated comprehensive kinetic model of hydrogen combustion. *International Journal of Chemical Kinetics*, 36:566–575, 2004.

A. Roux, L. Y. M. Gicquel, S. Reichstadt, N. Bertier, G. Staffelbach, F. Vuillot, and T. J. Poinsot. Analysis of unsteady reacting flows and impact of chemistry description in large eddy simulations of side-dump ramjet combustors. *Combustion and Flame*, 157:176–191, 2010.

V. Sankaran and S. Menon. Subgrid combustion modeling of 3-d premixed flames in the thin-reaction-zone regime. *Proceedings of the Combustion Institute*, 30:575–582, 2005.

J. E. Shepherd, S. Bane, and J. Ziegler. Development of one-step chemistry models for hydrogen-air and propane-air systems. Technical report, Graduate Aerospace Laboratories, California Institute of Technology, Pasadena, California, 2008. Report for FM Global.

S. Singh, D. Liberman, and J. E. Shepherd. Combustion behind shock waves. In *Fall 2003 Technical Meeting of the Western States Section of the Combustion Institute*, 2003. Paper 03F-29.

M. Thiele, J. Warnatz, and U. Maas. Geometrical study of spark ignition in two dimensions. *Combustion Theory and Modeling*, 4:413–434, 2000.

A   1D Flat Flames With One-Step Chemistry

A.1   1D Flat Flame Simulation

The Cantera Python demo *adiabatic_flame.py* calculates temperature and species profiles and flame speeds (laminar burning velocities) for freely-propagating flat flames with multicomponent transport properties. The code solves the 1D mass, species, and energy conservation equations,

$$\rho u = \rho_{in} S_u = \dot{m} = \text{constant} \tag{53}$$

$$\rho \frac{\partial Y_i}{\partial t} + \dot{m} \frac{\partial Y_i}{\partial z} = -\frac{\partial j_{i,z}}{\partial z} + \dot{\omega}_i W_i \tag{54}$$

$$\rho c_p \frac{\partial T}{\partial t} + \dot{m} c_p \frac{\partial T}{\partial z} = \frac{\partial}{\partial z} \left(\kappa \frac{\partial T}{\partial z} \right) - \sum_{i=1}^{N} c_{pi} j_{i,z} \frac{\partial T}{\partial z} - \sum_{i=1}^{N} h_i \dot{\omega}_i W_i \tag{55}$$

The solution algorithm uses pseudo-time stepping and a Newton iteration scheme to implicitly solve for the steady-state solution vector (temperature T and the species mass fractions Y_i) at each grid point in the domain. The flame speed (laminar burning velocity), related to $\dot{m}$ as shown in Equation 53, is calculated as part of the solution. Figure 24 illustrates the problem domain.
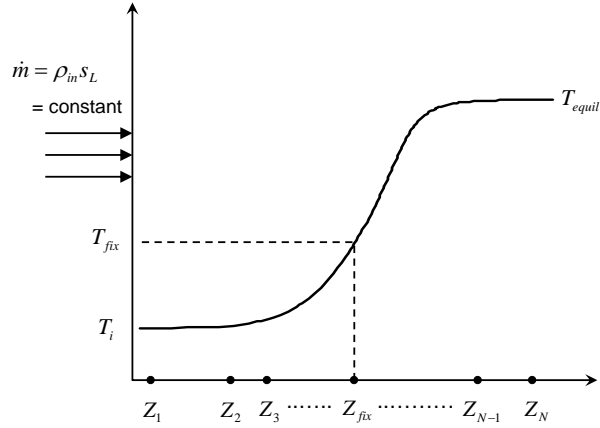
Figure 24: Problem domain for 1D flat flame calculation, with an example temperature profile shown. The flame is discretized into N grid points (at varying intervals), and the flame equations are solved for T, u, and Y_i at each grid point. The temperature is fixed at one interior grid point as part of the solution algorithm.

The pressure is assumed to be constant in the problem, so the density can be found from the temperature and the mass fractions using the ideal gas law,

$$p = \text{constant} = \rho R T \tag{56}$$

so

$$\rho = \frac{p}{RT} \tag{57}$$

where

$$R = \frac{\tilde{R}}{W_{mix}} = \frac{\tilde{R}}{\frac{1}{\sum_{i=1}^{N} \frac{Y_i}{W_i}}} \tag{58}$$

To solve the problem, the following initial/boundary conditions must be supplied:

1. Pressure (constant throughout problem)

2. Temperature of reactants (at the inlet to the flame structure)

3. Initial guess for mass flow rate, $\dot{m}$

4. Initial solution grid through the flame

5. Initial guess for temperature and species profiles on the initial grid

We also have to model the following terms in the conservation equations:

1. Specific heat of each species, c_{pi}

2. Thermal conductivity of the mixture, κ

3. Diffusive flux of each species, $j_{i,z}$

4. Enthalpy of each species, h_i

5. Net production rate of each species, $\dot{\omega}_i$

A.2   One-Step Reaction Model

The problem can be greatly simplified by making the assumption that all of the chemical kinetics can be simulated by a one-step global reaction

$$\text{Reactants (R)} \rightarrow \text{Products (P)}$$
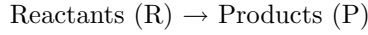
Making this assumption leads to the following simplifications:

1. $\displaystyle\sum_{i=1}^{N} Y_i = Y_R + Y_P = 1$ and therefore $Y_R = 1 - Y_P$

2. $\dot{\omega}_R = -\dot{\omega}_P$ (rate of production of product P is equal to the rate of consumption of reactant R)

3. $j_{i,z} = \rho Y_i V_i$ where V_i is the diffusion velocity of species i; but $\displaystyle\sum_{i=1}^{N} Y_i V_i = 0 = Y_R V_R + Y_P V_P$ which leads to $j_{R,z} = -j_{P,z}$

In this model we also assume that both the reactants and products have the same molecular properties, i.e.,

1. $c_{p,R} = c_{p,P}$

2. $W_R = W_P$

Using these simplifications in the species conservation relationship (Equation 54) reduces the number of equations to just one, since the parameters Y_i, $j_{i,z}$, W_i, and $\dot{\omega}_i$ of the two species can be related to each other. Writing the species conservation equation in terms of the mass fraction of the product, Y_P, gives,

$$\rho \frac{\partial Y_P}{\partial t} + \dot{m} \frac{\partial Y_p}{\partial z} = -\frac{\partial}{\partial z}\left(j_{P,z}\right) + \dot{\omega}_P W_P \tag{59}$$

It can be shown that the equation written in terms of the mass fraction of the reactant is completely equivalent. Now we use the simplifications in the energy conservation equation (Equation 55) to give

$$\rho c_p \frac{\partial T}{\partial t} + \dot{m} c_p \frac{\partial T}{\partial z} - \frac{\partial}{\partial z}\left(\kappa \frac{\partial T}{\partial z}\right) = -\left(h_R \dot{\omega}_R W_R + h_P \dot{\omega}_P W_P\right) \tag{60}$$

where

$$W_R \dot{\omega}_R = W_R\left(-k[R]\right) = -W_R k[R] \tag{61}$$

and

$$W_P \dot{\omega}_P = W_R k[R] \tag{62}$$

where k is the rate of the one step reaction $R \rightarrow P$. The concentration of a species can be expressed in terms of the mass fraction,

$$[i] = \frac{\rho Y_i}{W_i}. \tag{63}$$

Substituting in the expressions for $\dot{\omega}_R$ and $\dot{\omega}_P$ and using Equation 63, the right hand side of the energy equation (Equation 60) becomes

$$-\left(h_R W_R \dot{\omega}_R + h_P W_P \dot{\omega}_P\right) = -\left(-kW_R \frac{\rho Y_R}{W_R} h_R + kW_P \frac{\rho Y_R}{W_R} h_P\right) = -\rho Y_R\left(h_P - h_R\right)k. \tag{64}$$

Replacing Y_R with $1 - Y_P$ gives the final form of the energy equation for the one-step reaction model

$$\rho c_p \frac{\partial T}{\partial t} + \dot{m} c_p \frac{\partial T}{\partial z} - \frac{\partial}{\partial z}\left(\kappa \frac{\partial T}{\partial z}\right) = -\rho\left(1 - Y_P\right)\left(h_P - h_R\right)k. \tag{65}$$

The equations for species (Equation 59) and energy (Equation 65) can also be formulated in terms one variable, called the "progress variable" λ, which in this case we set equal to the mass fraction of the product, Y_P. Therefore $\lambda = 0$ at the start of the reaction (no product P) and $\lambda = 1$ at the end (all product P). Substituting $Y_P = \lambda$ into Equation 59 gives

$$\rho \frac{\partial \lambda}{\partial t} + \dot{m} \frac{\partial \lambda}{\partial z} = -\frac{\partial j_{,z}}{\partial z} + \dot{\omega}_P W_P. \tag{66}$$

But recall from our analysis of the energy equation, we found that

$$\dot{\omega}_P W_P = \rho Y_R k = \rho\left(1 - Y_P\right)k = \rho\left(1 - \lambda\right)k \tag{67}$$

so

$$\rho \frac{\partial \lambda}{\partial t} + \dot{m} \frac{\partial \lambda}{\partial z} = -\frac{\partial j_{,z}}{\partial z} + \rho\left(1 - \lambda\right)k \qquad \underline{\text{Species Conservation}} \tag{68}$$

Substituting λ into the energy equation gives

$$\rho c_p \frac{\partial T}{\partial t} + \dot{m} c_p \frac{\partial T}{\partial z} - \frac{\partial}{\partial z}\left(\kappa \frac{\partial T}{\partial z}\right) = -\rho\left(1 - \lambda\right)\left(h_P - h_R\right)k \qquad \underline{\text{Energy Conservation}} \tag{69}$$

B Effective Reaction Orders and Activation Energies for Hydrogen-Air Systems

Table 2 lists the values of effective reaction order n and activation energy E_a calculated for a range of hydrogen-air compositions using the constant pressure explosion method with reaction order dependence (Equations 17 and 22). The pressure is 1 bar, and the initial temperature used in the explosion calculations was $T_0 = 0.9T_b$ where T_b is the adiabatic flame temperature found by equilibrating the mixture at constant pressure and enthalpy. The temperature and density intervals used for the derivatives were $T' = 30$ K and $\rho' = 1.1\rho_0$, respectively. The unburned temperature is 300 K and the adiabatic flame temperature T_b was used for the burned gas temperature in calculating the Zeldovich number.

Table 3 lists the values of effective activation energy E_a calculated for a range of hydrogen-air compositions using the constant pressure explosion method with constant volume initial conditions (Equation 26). The initial pressure is 1 bar, and the initial temperature used in the explosion calculations was $T_0 = 0.9T_b$ where T_b is the adiabatic flame temperature found by equilibrating the mixture at constant pressure and enthalpy. The temperature interval used for the derivative was $T' = 30$ K. The unburned temperature is 300 K and the adiabatic flame temperature T_b was used for the burned gas temperature in calculating the Zeldovich number.

Table 4 lists the values of effective activation energy E_a calculated for a range of hydrogen-air compositions using the constant volume explosion method (Equation 31). The initial pressure is 1 bar, and the initial temperature used in the explosion calculations was $T_0 = 0.9T_b$ where T_b is the adiabatic flame temperature found by equilibrating the mixture at constant pressure and enthalpy. The temperature interval used for the derivative was $T' = 30$ K. The unburned temperature was 300 K and the constant volume explosion temperature, found by equilibrating the mixture at constant volume and energy, was used in this case for the burned gas temperature for calculating the Zeldovich number.

Table 2: Effective Reaction Orders and Activation Energies Calculated Using the Constant Pressure Explosion Method with Reaction Order Dependence (Equations 17 and 22).

%H_2	n	β	E_a (kcal/mol)
70	1.8	6.3	21.602
65	1.9	6.0	22.173
60	2.0	5.7	22.862
55	1.9	5.5	23.358
50	1.8	5.3	24.131
45	1.8	5.0	24.305
40	1.8	5.1	26.061
35	1.8	4.9	26.181
30	1.8	5.1	27.856
25	2.0	4.3	21.425
20	1.9	5.0	21.806
15	1.9	5.5	20.263
14	1.9	5.7	20.176
13	1.9	5.8	20.017
12	1.8	6.3	20.308

Table 3: Effective Activation Energies Calculated Using the Constant Pressure Explosion Method with Constant Volume Initial Conditions (Equation 26).

$\%\mathrm{H}_2$	β	E_a (kcal/mol)
70	6.3	21.435
65	5.9	21.961
60	5.7	22.968
55	5.3	22.863
50	5.4	24.841
45	5.0	24.084
40	5.2	26.702
35	5.1	27.422
30	5.2	28.359
25	4.2	20.765
20	5.0	21.759
15	5.5	20.250
14	5.7	20.259
13	5.8	20.009
12	6.2	20.211

Table 4: Effective Activation Energies Calculated Using the Constant Volume Explosion Method (Equation 31).

%H_2	β	E_a (kcal/mol)
70	5.3	21.174
65	4.9	21.285
60	4.7	22.071
55	4.7	23.717
50	4.7	25.253
45	4.4	24.934
40	4.7	27.566
35	4.6	28.277
30	4.9	30.460
25	3.5	20.373
20	4.2	21.313
15	4.7	20.058
14	4.8	19.938
13	5.0	19.777
12	5.4	20.079

C   Sensitivity of Effective Activation Energy to Flamespeed

The basic theory of the flame speed method for calculating the effective activation energy as presented by FM Global (Bauwens, 2007) and discussed in (Shepherd et al., 2008) is that the activation energy can be estimated using the sensitivity of the flame speed to small changes in the initial temperature and pressure. To assess the validity of this approach, we investigated the dependence of the flame speed on initial temperature and pressure using two different values for the activation energy. If the activation energy is in fact dependent on the flame speed sensitivity to temperature and pressure, we would expect to see a change in the slopes of the flame speed versus temperature and pressure curves for the two different activation energies.

We have previously calculated the flame speed versus small changes in the initial temperature and pressure using a second order one-step model for a 30% hydrogen mixture, as discussed in Section 6.2. The effective activation energy used was the value calculated from the constant pressure explosion method, $E_a = 27.856$ kcal/mol and the pre-exponential factor A was 5.80×10^{14}. We then doubled the activation energy to $E_a = 55.712$ kcal/mol and found a new value of the pre-exponential factor to match the one-step flamespeed to the full chemistry at 300 K and 1 bar, $A = 1.35 \times 10^{18}$. We then calculated the flamespeed with initial temperatures increasing from 290 K to 400 K by 10 K with pressure fixed at 1 bar, and with initial pressures increasing from 0.85 bar to 1.5 bar by 0.05 bar with temperature fixed at 300 K.

The flame speed versus initial temperature calculated using full chemistry, the second order one-step model with $E_a = 27.856$ kcal/mol, and with the second order one-step model with $E_a = 55.712$ kcal/mol is shown in Figure 25(a). For initial temperatures of 280 K to 350 K the flame speed results from the two one-step models with different activation energies match to within 4% and for inititial temperatures from 360 K to 400 K the two results match to within 6 to 16%. The slopes of the flamespeed curves, estimated using the average of the forward and backward differences, are plotted in Figure 25(b). The slopes of the flamespeed versus initial temperature curves calculated using the two different activation energies are very close (within 2 to 15% of eachother) for several initial temperatures, i.e. 300, 310, 320, 340, and 400 K, and differ by more than 30% for other initial temperatures. However, there is no consistent significant difference in the slopes of the flamespeed versus temperature curves for the two different activation energies. The flamespeed versus small changes in initial pressure is shown in Figure 26(a) with values calculated using full chemistry and the second order one-step models with $E_a = 27.856$ kcal/mol and with $E_a = 55.712$ kcal/mol. For all three cases the flamespeed is approximately constant for small changes in initial pressure (0.85 to 1.50 bar) and there is no apparent difference in the slopes of the curves calculated using the one-step models with two different activation energies. The slopes of the flamespeed versus initial pressure curves, estimated once again using the average of forward and backward differences, are plotted in Figure 26(b). The slopes from the two one-step model calculations both oscillate around zero, as expected for a one-step model with $n = 2$. While the sensitivities of the flamespeed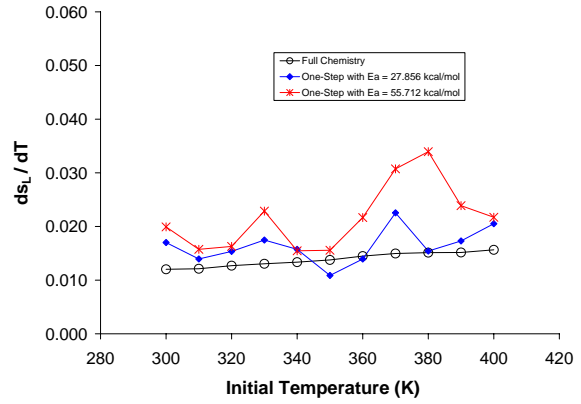 to small changes in the initial temperature and pressure are not numerically identical for the two different activation energies, in this example there is no consistent difference in the flamespeed dependence that can be identified and attributed to the differing values of E_a. Therefore, it does not appear that the activation energy is sensitive enough to the flamespeed dependence on small changes in the initial conditions to use the flamespeed to extract an effective value of E_a.
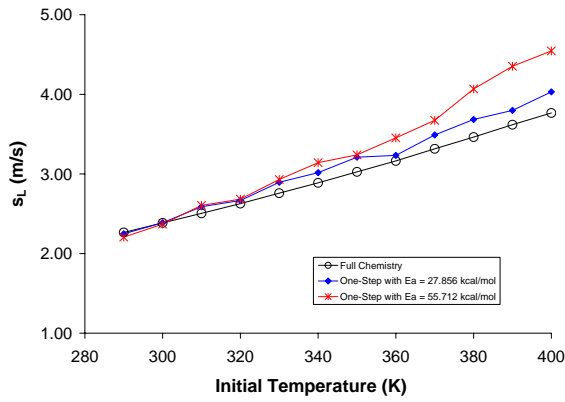
(a)   (b)

Figure 25: Flamespeed versus small changes in initial temperature calculated using full chemistry and one-step models with two different activation energies (a) and the slopes of the flame speed curves (b).
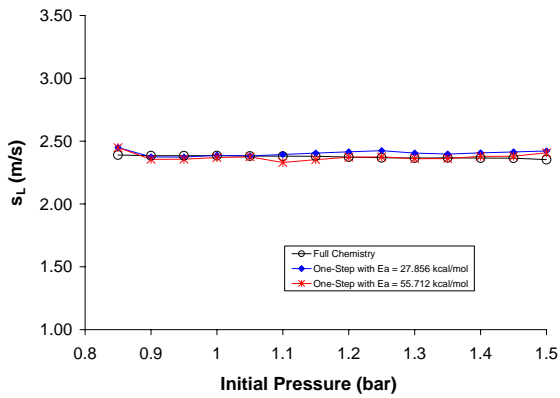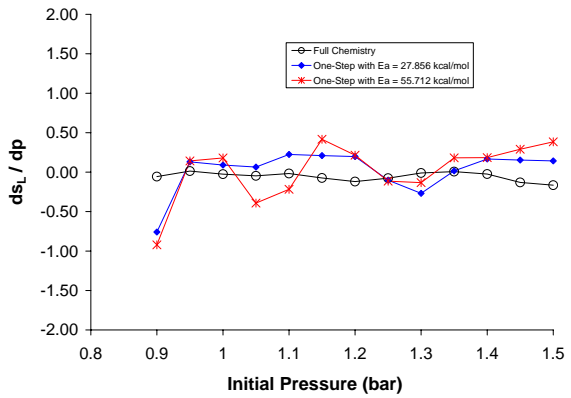
(a)   (b)

Figure 26: Flamespeed versus small changes in initial pressure calculated using full chemistry and one-step models with two different activation energies (a) and the slopes of the flame speed curves (b).

D Python 1D Adiabatic Flame Code

```
#
# ONESTEP_FLAME - A freely-propagating, adiabatic, premixed
#          flat (1D) flame using a one step chemistry model.
#
from Cantera import *
from Cantera.OneD import *
from Cantera.OneD.FreeFlame import FreeFlame


####################################################################
#
# parameter values
#
p          =   100000              # pressure
tin        =   300                 # unburned gas temperature

comp = 'R:1, P:0'  # premixed gas composition
                   # R = reactant, P = product

initial_grid = [0.0, 0.001, 0.01, 0.02, 0.029, 0.03] # meters

tol_ss    = [1.0e-5, 1.0e-9]       # [rtol atol] for steady-state
                                   # problem
tol_ts    = [1.0e-5, 1.0e-9]       # [rtol atol] for time stepping

loglevel  = 1                      # amount of diagnostic output (0
                                   # to 5)

refine_grid = 1                    # 1 to enable refinement, 0 to
                                   # disable

gas = importPhase('onestep.cti')  # use one step model input (.cti) file

# set the gas state to the unburned state
gas.setState_TPX(tin, p, comp)

# initialize the flame object
f = FreeFlame(gas = gas, grid = initial_grid, tfix = 600.0)

# set the upstream properties
f.inlet.set(mole_fractions = comp, temperature = tin)

f.set(tol = tol_ss, tol_time = tol_ts)
f.showSolution()

# solve without the energy equation
f.set(energy = 'off')
f.setRefineCriteria(ratio = 10.0, slope = 1, curve = 1)
f.setMaxJacAge(50, 50)
f.setTimeStep(1.0e-5, [1, 2, 5, 10, 20])

f.solve(loglevel, refine_grid)
f.save('ch4_adiabatic.xml','no_energy',
```

```
            'solution with the energy equation disabled')

# solve with the energy equation
f.set(energy = 'on')
f.setRefineCriteria(ratio = 3.0, slope = 0.1, curve = 0.2)
f.solve(loglevel, refine_grid)
f.save('ch4_adiabatic.xml','energy',
        'solution with the energy equation enabled')
print 'mixture-averaged flamespeed = ',f.u()[0]


# write the velocity, temperature, density, and mole fractions to a CSV file
z = f.flame.grid()
T = f.T()
u = f.u()
V = f.V()
fcsv = open('onestep_flame.csv','w')
writeCSV(fcsv, ['z (m)', 'u (m/s)', 'V (1/s)', 'T (K)', 'rho (kg/m3)']
          + list(gas.speciesNames()))
for n in range(f.flame.nPoints()):
    f.setGasState(n)
    writeCSV(fcsv, [z[n], u[n], V[n], T[n], gas.density()]
             +list(gas.moleFractions()))
fcsv.close()

# print the laminar flame speed and flame temperature to the output
# screen
print 'solution saved to onestep_flame.csv'
print 'multicomponent flamespeed = ',u[0]
print 'flame temperature = ', T[n-1]
f.showStats()
```

E One-Step Model Parameters for Hydrogen-Air Systems

Table 5 lists first order ($n = 1$) one-step model values for activation energy E_a, pre-exponential factor A, heat release q and corresponding constant $(a_5)_P$ used in the Cantera input (.cti) file for a range of hydrogen-air compositions. The activation energies were found using the constant pressure explosion method (Equation 22) with effective reaction orders also found from the constant pressure explosion method (Equation 17), the heat release values were found directly from the flame temperature, and the pre-exponential factors were obtained through iteration.

Table 5: First Order ($n = 1$) One-Step Model Parameters for Hydrogen-Air Systems

%H$_2$	E_a (kcal/mol)	A (1/s)	$(a_5)_P$	q (kJ/mol)
70	21.602	4.080E+09	-3338	21.56
65	22.173	4.790E+09	-3712	24.66
60	22.862	5.150E+09	-4084	27.76
55	23.358	4.860E+09	-4448	30.78
50	24.131	4.740E+09	-4812	33.81
45	24.305	3.550E+09	-5170	36.79
40	26.061	4.040E+09	-5522	39.71
35	26.181	2.330E+09	-5847	42.41
30	27.856	2.260E+09	-5972	43.46
25	21.425	3.580E+08	-5355	38.33
20	21.806	3.450E+08	-4493	31.16
15	20.263	8.200E+07	-3579	23.56
14	20.176	5.510E+07	-3398	22.06
13	20.017	3.110E+07	-3216	20.54
12	20.308	1.185E+07	-2984	18.61

Table 6 lists second order ($n = 2$) one-step model values for activation energy E_a, pre-exponential factor A, heat release q and corresponding constant $(a_5)_P$ used in the Cantera input (.cti) file for a range of hydrogen-air compositions. The activation energies were found using the constant pressure explosion method (Equation 22) with effective reaction orders also found from the constant pressure explosion method (Equation 17), the heat release values were found directly from the flame temperature, and the pre-exponential factors were obtained through iteration.

Table 6: Second Order ($n = 2$) One-Step Model Parameters for Hydrogen-Air Systems

%H_2	E_a (kcal/mol)	A (m^3/mol·s)	$(a_5)_P$	q (kJ/mol)
70	21.602	7.000E+14	-3338	21.56
65	22.173	8.800E+14	-3712	24.66
60	22.862	9.960E+14	-4084	27.76
55	23.358	1.010E+15	-4448	30.78
50	24.131	1.027E+15	-4812	33.81
45	24.305	7.940E+14	-5170	36.79
40	26.061	9.970E+14	-5522	39.71
35	26.181	5.690E+14	-5847	42.41
30	27.856	5.870E+14	-5972	43.46
25	21.425	7.110E+13	-5355	38.33
20	21.806	6.580E+13	-4493	31.16
15	20.263	1.350E+13	-3579	23.56
14	20.176	8.750E+12	-3398	22.06
13	20.017	4.610E+12	-3216	20.54
12	20.308	1.820E+12	-2984	18.61

F   Second Order One-Step Model Cantera Input (.cti) File

Below is an example Cantera input (.cti) file using second order one-step model parameters for 30% hydrogen-air.

```
# ONE-STEP MODEL FOR HYDROGEN-AIR WITH PHI=1.02
# 2nd ORDER REACTION WITH ARGON ATOMS
#
# Generated from file argon.inp
# by ck2cti on Mon Aug 25 09:52:59 2003
#
# Transport data from file ../transport/gri30_tran.dat.

units(length = "cm", time = "s", quantity = "mol", act_energy = "cal/mol")


ideal_gas(name = "gas",
      elements = " Ar ",
      species = """ R P """,
      reactions = "all",
      transport = "Mix",
      initial_state = state(temperature = 300,
                      pressure = OneAtm)    )




#-------------------------------------------------------------------------------
#  Species data
#-------------------------------------------------------------------------------

species(name = "R",
    atoms = " Ar:1 ",
    thermo = (
       NASA( [  300.00,  1000.00], [  2.5000000000E+00,   0.000000000E+00,
                0.000000000E+00,   0.000000000E+00,   0.000000000E+00,
               -7.453750000E+02,   4.379674910E+00] ),
       NASA( [ 1000.00,  5000.00], [  2.5000000000E+00,   0.000000000E+00,
                0.000000000E+00,   0.000000000E+00,   0.000000000E+00,
               -7.453750000E+02,   4.379674910E+00] )
             ),
    transport = gas_transport(
                     geom = "atom",
                     diam =      3.33,
                     well_depth =   136.50),
    note = "120186"
       )

species(name = "P",
    atoms = " Ar:1 ",
    thermo = (
       NASA( [  300.00,  1000.00], [  2.5000000000E+00,   0.000000000E+00,
                0.000000000E+00,   0.000000000E+00,   0.000000000E+00,
```

```
                         -5.972000000E+03,   4.379674910E+00] ),
         NASA( [ 1000.00,  5000.00], [  2.5000000000E+00,   0.000000000E+00,
                 0.000000000E+00,   0.000000000E+00,   0.000000000E+00,
                 -5.972000000E+03,   4.379674910E+00] )
              ),
     transport = gas_transport(
                    geom = "atom",
                    diam =     3.33,
                    well_depth =   136.50),
     note = "5"
        )




#-------------------------------------------------------------------------------
#  Reaction data
#-------------------------------------------------------------------------------

#  Reaction 1
reaction( "R + R => P + P",   [5.870E+14, 0, 27856])
```

G   Cantera Python Code *STFLAME1.py* for Simulating a Flat Flame in a Strained Flow Field

This is the Cantera code used in examining the flame response to straining, applied to a mixture of 15% hydrogen in air ($\phi = 0.42$).

```
#
# STFLAME1 - A detached flat flame stabilized at a stagnation point
#

#    This script simulates a lean hydrogen-oxygen flame stabilized in
#    a strained flow field at an axisymmetric stagnation point on a
#    non-reacting surface. The solution begins with a flame attached
#    to the inlet (burner), and the mass flow rate is progressively
#    increased, causing the flame to detach and move closer to the
#    surface. This example illustrates use of the new 'prune' grid
#    refinement parameter, which allows grid points to be removed if
#    they are no longer required to resolve the solution. This is
#    important here, since the flame front moves as the mass flowrate
#    is increased. Without using 'prune', a large number of grid
#    points would be concentrated upsteam of the flame, where the
#    flamefront had been previously. (To see this, try setting prune
#    to zero.)

from Cantera import *
from Cantera.OneD import *
from Cantera.OneD.StagnationFlow import StagnationFlow

#################################################################
#
# parameter values
#
p         =   OneAtm           # pressure
tburner   =   301                   # burner temperature
tsurf     =   302

# each mdot value will be solved to convergence, with grid refinement,
# and then that solution will be used for the next mdot

mdot      =   [0.1, 0.5, 1.0, 1.5, 2, 2.5, 2.6, 2.7, 2.8, 2.9, 3, 3.1, 3.2, 3.3, 3.4, 3.5]      # kg/m^2

comp      =   'H2:0.42, O2:0.5, N2:1.88'  # premixed gas composition

# The solution domain is chosen to be 50 cm, and a point very near the
# downstream boundary is added to help with the zero-gradient boundary
# condition at this boundary.

initial_grid = [0.0, 0.0001, 0.001, 0.002, 0.003, 0.005,
                0.0059, 0.006];

tol_ss    = [1.0e-4, 1.0e-12]        # [rtol atol] for steady-state
                                     # problem
tol_ts    = [1.0e-3, 1.0e-8]         # [rtol atol] for time stepping
```

```
loglevel  = 1                          # amount of diagnostic output (0
                                       # to 5)


refine_grid = 1                        # 1 to enable refinement, 0 to
                                       # disable

ratio = 5.0
slope = 0.1
curve = 0.2
prune = 0.05




############### create the gas object ######################
#
# This object will be used to evaluate all thermodynamic, kinetic,
# and transport properties
#

#gas = IdealGasMix(rxnmech)
gas = importPhase('Lietal_mech_2003.cti','gas')
# set its state to that of the unburned gas at the burner
gas.setState_TPX(tburner, p, comp)

# Create the stagnation flow object with a non-reactive surface.  (To
# make the surface reactive, supply a surface reaction mechanism.  see
# example catcomb.py for how to do this.)
f = StagnationFlow(gas = gas, grid = initial_grid)

# set the properties at the inlet
f.inlet.set(massflux = mdot[0], mole_fractions = comp, temperature = tburner)

# set the surface state
f.surface.setTemperature(tsurf)

f.set(tol = tol_ss, tol_time = tol_ts)
f.setMaxJacAge(5, 10)
f.set(energy = 'off')
f.init(products = 'equil') # assume adiabatic equilibrium products
f.showSolution()

f.solve(loglevel, refine_grid)

f.setRefineCriteria(ratio = ratio, slope = slope,
                    curve = curve, prune = prune)
f.set(energy = 'on')

m = 0
for md in mdot:
    f.inlet.set(mdot = md)
    f.solve(loglevel,refine_grid)
    m = m + 1
    f.save('stflame1.xml','mdot'+'m','mdot = '+'md'+' kg/m2/s')
```

```
    # write the velocity, temperature, and mole fractions to a CSV file
    z = f.flow.grid()
    T = f.T()
    u = f.u()
    V = f.V()
    fcsv = open('stflame1_'+`m`+'.csv','w')
    writeCSV(fcsv, ['z (m)', 'u (m/s)', 'V (1/s)', 'T (K)']
            + list(gas.speciesNames()))
    for n in range(f.flow.nPoints()):
        f.setGasState(n)
        writeCSV(fcsv, [z[n], u[n], V[n], T[n]]+list(gas.moleFractions()))
    fcsv.close()

    print 'solution saved to flame1.csv'

f.showStats()
```

H   4-Species One-Step Model Cantera Input (.cti) File

This is the Cantera input (.cti) file for the 4-species one-step model for a mixture of 15% hydrogen-air with
Le = 0.42.

```
# ONE-STEP MODEL FOR 15% HYDROGEN-AIR
# 2nd ORDER REACTION WITH 4 SPECIES
# AND ACCURATE TRANSPORT PARAMETERS

units(length = "cm", time = "s", quantity = "mol", act_energy = "cal/mol")

ideal_gas(name = "gas",
      elements = " H O N ",
      species = """ H2 H2O O2 N2 """,
      reactions = "all",
      transport = "Mix",
      initial_state = state(temperature = 300,
                            pressure = OneAtm)    )



#-------------------------------------------------------------------------------
#  Species data
#-------------------------------------------------------------------------------

species(name = "H2",
    atoms = " H:2 ",
    thermo = (
       NASA( [  300.00,  1000.00], [  1.5000000000E+01,   0.000000000E+00,
                0.000000000E+00,   0.000000000E+00,   0.000000000E+00,
               -7.453750000E+02,   4.379674910E+00] ),
       NASA( [ 1000.00,  5000.00], [  1.5000000000E+01,   0.000000000E+00,
                0.000000000E+00,   0.000000000E+00,   0.000000000E+00,
               -7.453750000E+02,   4.379674910E+00] )
             ),
    transport = gas_transport(
                   geom = "linear",
                   diam =      2.92,
                   well_depth =     38.00,
                   polar =     0.79,
                   rot_relax =   280.00),
    note = "121286"
       )

species(name = "O2",
    atoms = " O:2 ",
    thermo = (
       NASA( [  300.00,  1000.00], [  1.5000000000E+01,   0.000000000E+00,
                0.000000000E+00,   0.000000000E+00,   0.000000000E+00,
               -7.453750000E+02,   4.379674910E+00] ),
       NASA( [ 1000.00,  5000.00], [  1.5000000000E+01,   0.000000000E+00,
                0.000000000E+00,   0.000000000E+00,   0.000000000E+00,
               -7.453750000E+02,   4.379674910E+00] )
             ),
    transport = gas_transport(
```

```
                                geom = "linear",
                                diam =       3.46,
                                well_depth =   107.40,
                                polar =       1.60,
                                rot_relax =       3.80),
        note = "121386"
            )


species(name = "H2O",
        atoms = " H:1 O:1 ",
        thermo = (
           NASA( [  300.00,  1000.00], [  1.5000000000E+01,   0.000000000E+00,
                    0.000000000E+00,   0.000000000E+00,   0.000000000E+00,
                   -3.087000000E+04,   4.379674910E+00] ),
           NASA( [ 1000.00,  5000.00], [  1.5000000000E+01,   0.000000000E+00,
                    0.000000000E+00,   0.000000000E+00,   0.000000000E+00,
                   -3.087000000E+04,   4.379674910E+00] )
                 ),
        transport = gas_transport(
                        geom = "nonlinear",
                        diam =       2.61,
                        well_depth =   572.40,
                        dipole =       1.84,
                        rot_relax =       4.00),
        note = "20387"
            )


species(name = "N2",
        atoms = " N:2 ",
        thermo = (
           NASA( [  300.00,  1000.00], [ 3.298677000E+000,  1.408240000E-003,
                   -3.963222000E-006,  5.641515000E-009, -2.444855000E-012,
                   -1.020900000E+003,  3.950372000E+000] ),
           NASA( [ 1000.00,  5000.00], [ 2.926640000E+000,  1.487977000E-003,
                   -5.684761000E-007,  1.009704000E-010, -6.753351000E-015,
                   -9.227977000E+002,  5.980528000E+000] )
                 ),
        transport = gas_transport(
                        geom = "linear",
                        diam =       3.62,
                        well_depth =    97.53,
                        polar =       1.76,
                        rot_relax =       4.00),
        note = "121286"
            )


#-------------------------------------------------------------------------------
#  Reaction data
#-------------------------------------------------------------------------------

#  Reaction 1
reaction( "H2 + O2 => H2O + H2O",   [2.85E+14, 0, 20263])
```